energies

MDPI

Review

Research Progress on Convective Heat Transfer Characteristics of Supercritical Fluids in Curved Tube

Xinxin Liu [1,2], Shuoshuo Li [1,2], Liang Liu [1,2], Chao He [1,2], Zhuang Sun [3], Faruk Özdemir [4], Muhammad Aziz [3] and Po-Chih Kuo [3,*]

[1] Key Laboratory of New Materials and Facilities for Rural Renewable Energy of Ministry of Agriculture and Rural Affairs, Collaborative Innovation Center of Biomass Energy, College of Mechanical & Electrical Engineering, Henan Agricultural University, Zhengzhou 450002, China
[2] Henan International Joint Laboratory of Biomass Energy and Nanomaterials, Henan Agricultural University, Zhengzhou 450002, China
[3] Institute of Industrial Science, The University of Tokyo, 4-6-1 Komaba, Meguro-ku, Tokyo 153-8505, Japan
[4] Process and Energy Department, Faculty of 3mE, Delft University of Technology, 2628 CB Delft, The Netherlands
* Correspondence: pckuo225@gmail.com or pckuo@iis.u-tokyo.ac.jp

Abstract: Because of their compact structure, ease of processing and higher heat transfer coefficient, curved-tube heat exchangers are widely applied in various industry applications, such as nuclear power systems, solar-powered engineering, aircraft engine cooling systems and refrigeration and cryogenic systems. Accurate knowledge about the heat transfer characteristics of the supercritical fluids in the tube is critical to the design and optimization of a curved-tube heat exchanger. The available literature indicates that the flow of supercritical fluids flowing in curved tubes affected by the dual effects of the buoyancy force and centrifugal force is more complex compared to straight tubes. Therefore, to obtain insight into their unique characteristics and further research progress, this paper presents a comprehensive review of available experimental and numerical research works on fluids at supercritical pressure flowing in curved tubes. Overall, the secondary flow caused by the curvature enhances the heat transfer and delays the heat transfer deterioration, but it also causes a non-uniform heat transfer distribution along the circumferential direction, and the strengthening performance of the curved tube is damaged. Compared with the more mature theories regarding straight tubes, the flow structure, the coupling mechanism of buoyancy and centrifugal force, and the general heat transfer correlation of supercritical fluids in a curved tube still urgently need to be further studied. Most importantly, studies on the suppression of heat transfer oscillations and heat transfer inhomogeneities specific to curved tubes are scarce. Considering the current status and shortcomings of existing studies, some study topics for supercritical fluids in a curved tube are proposed.

Keywords: heat transfer characteristics; supercritical fluids; curved tube; heat transfer enhancement; buoyancy force; centrifugal force

Citation: Liu, X.; Li, S.; Liu, L.; He, C.; Sun, Z.; Özdemir, F.; Aziz, M.; Kuo, P.-C. Research Progress on Convective Heat Transfer Characteristics of Supercritical Fluids in Curved Tube. *Energies* **2022**, *15*, 8358. https://doi.org/10.3390/en15228358

Academic Editor: Abu-Siada Ahmed

Received: 19 September 2022
Accepted: 7 November 2022
Published: 9 November 2022

1. Introduction

In recent decades, supercritical fluids have been widely used in various power generation systems because of their extraordinary thermal properties [1–5]. Supercritical fluids can be regarded as at the intermediate state between liquid and vapor states: the bulk temperature increase from lower than pseudo-critical temperature to higher than pseudo-critical temperature is accompanied by thermos-physical properties changing drastically from the subcritical region to the supercritical region without phase change. Examples of the thermos-physical properties of CO_2 at various pressures are plotted against the temperature near pseudo-critical temperature (Figure 1). As shown in Figure 1, in the region away from the pseudo-critical point (low-enthalpy and high-enthalpy regions), the

variation in each property with temperature is small and decreases as one moves away from the critical point. In contrast, near the pseudo-critical point (high-enthalpy region), a 1 K temperature change leads to a several-fold decrease in density, viscosity and thermal conductivity, while the specific heat forms a peak at the pseudo-critical point that is tens of times larger than in the low-enthalpy and high-enthalpy regions.

Since 1950, supercritical water has been applied in traditional electric plants to improve thermal efficiency [6–9]. Supercritical water-cooled reactor Generation IV nuclear power plants have a high overall thermal efficiency of about 33–35% to about 45% due to their high operating pressure and temperature [10]. Similarly, supercritical CO_2 has widespread applications in fields such as nuclear reactor cooling systems, solar thermal power systems and trans-critical CO_2 heat pumps. The study [11] confirmed that the solar collector thermal efficiency with CO_2 as working fluid is higher than that of solar collectors using water, and the heat transfer efficiency can approach 60%. To obtain the optimal energy utilization, power generation systems with organic Rankine cycles for low-grade thermal energy (80–200 °C) conversion have attracted wide attention, and the heat transfer behaviors of organic fluids at supercritical pressure (such as R245fa, R1233zd(E)) were experimentally investigated [12,13]. Additionally, in recent years, with the rapid development of spaceflight and aviation technology, the flow and heat transfer performance of hydrocarbon fuels have also been receiving increased attention [14–18].

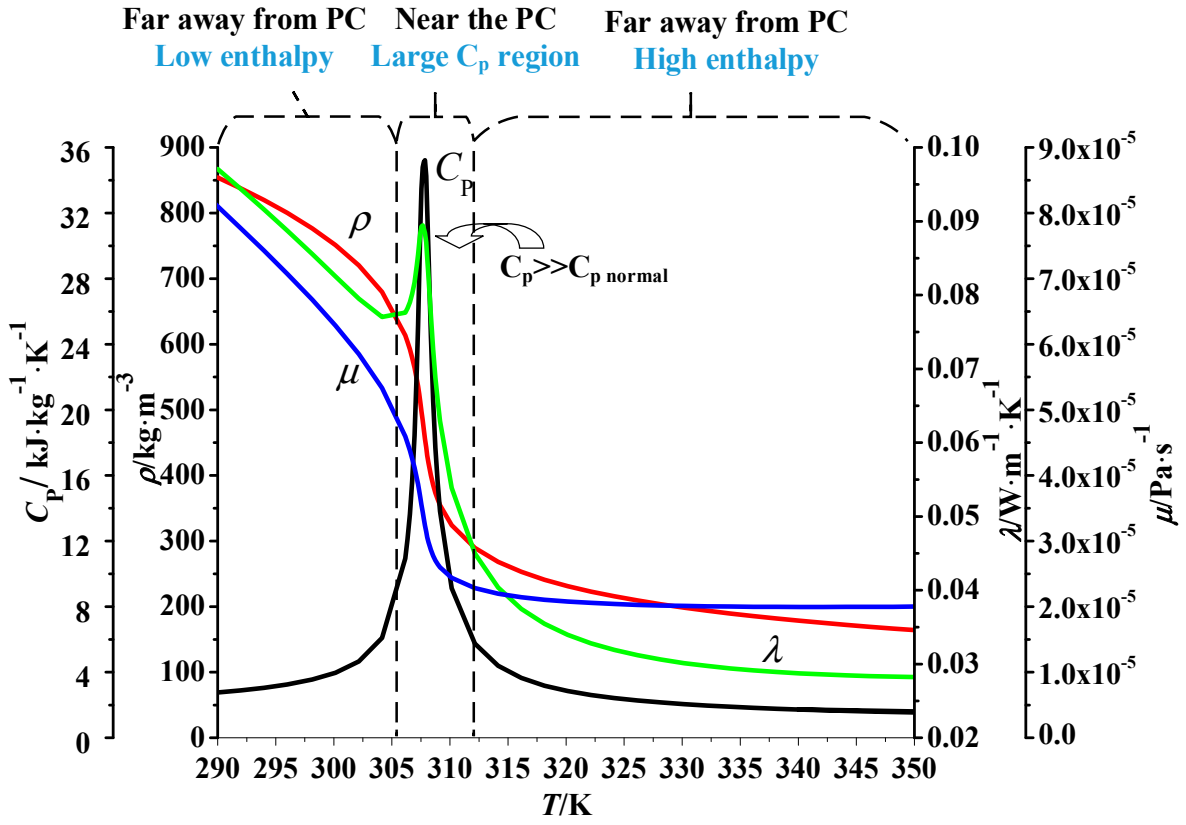

Figure 1. Thermo-physical properties of CO_2 at 8 MPa [19].

Figure 2 presents the relevant engineering applications of supercritical fluids in various fields [1,2,20–22]. The performance of heat exchangers in these engineering systems is of great importance to the efficiency, stability and safety of the systems. Accordingly, accurate knowledge about the heat transfer characteristics of the supercritical fluids in tubes is critical to the design and optimization of heat exchangers. Since the physical properties of supercritical fluids change drastically near the critical point, it is difficult to apply the flow heat transfer experimental data summarized for normal physical fluids [23,24]. Hence,

the flow and heat transfer characteristics of different conditions and flow directions in straight pipes have been frequently studied by domestic and foreign scholars through experiments and numerical simulations. The literature shows that convective heat transfer of supercritical fluids has three conditions [25,26]: normal heat transfer, heat transfer intensification, and heat transfer deterioration. The deterioration of heat transfer is usually accompanied by a sudden increase in the pipe wall temperature and a sharp decrease in the heat transfer capacity, which can be a great danger to the safe operation and efficiency of the heat exchanger and the whole system [27,28]. In the last decade, based on the certain understanding of heat transfer characteristics in smooth straight tubes, many scholars have carried out research on the heat transfer characteristics of supercritical fluids in enhanced tubes, with a view to providing a scientific and theoretical basis for suppressing heat transfer deterioration and improving high-efficiency supercritical heat exchangers.

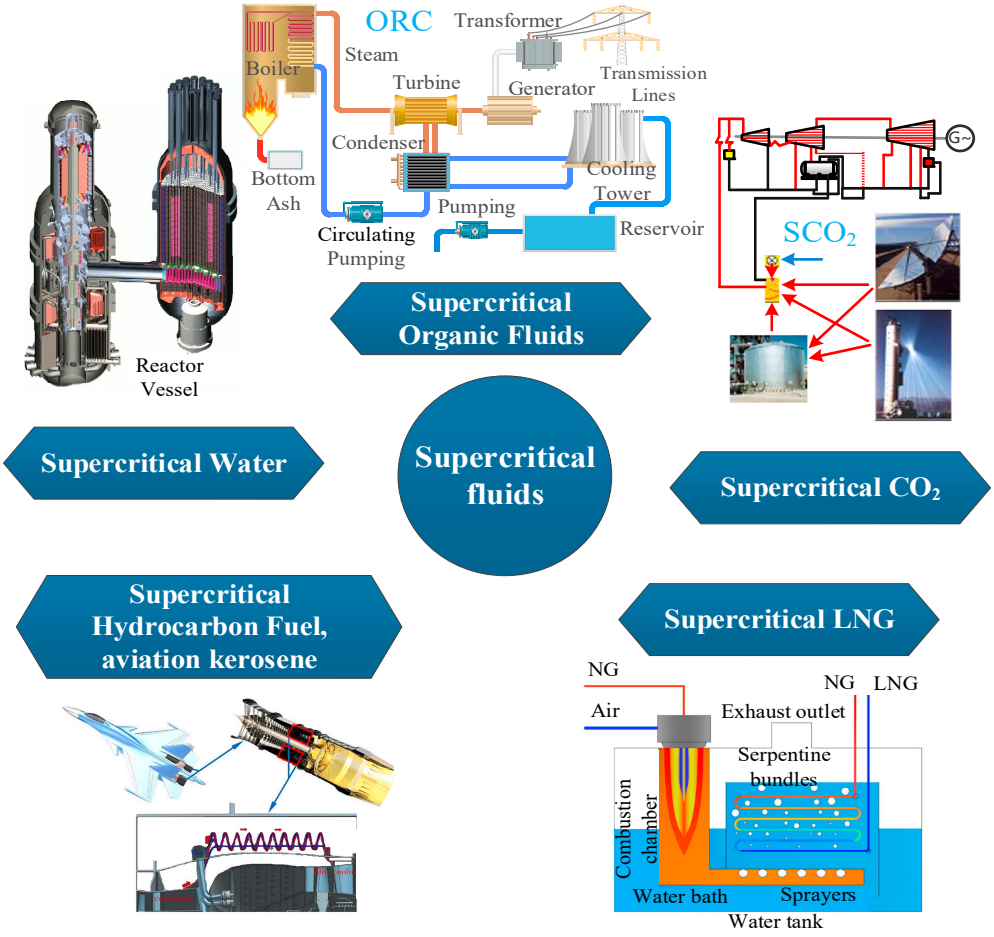

Figure 2. Examples of applications of supercritical fluids in various fields.

In general, various turbulence-enhancing devices such as curved tubes [29–33], ribs [34–40], twisted tapes [41,42] and metal foam [43,44] can increase the heat transfer coefficient. Among these passive methods, the technique of curved tubes has garnered much research attention. A curved tube is generally made from a straight seamless steel tube. The straight pipe is first subjected to a second cold rolling, a cold drawing deformation, normalized and tempered heat treatment processes, and surface inspection to ensure there are no cracks or warpage defects. Then, the qualified straight tube is curled by multi-head spiral coiler and space bender, and it then undergoes multiple finishing processes, i.e., external surface shot blasting, vacuum stress relief heat treatment, surface oxidation treatment and surface immersion treatment. It is then removed for cooling and drying, and the whole process is over. Therefore, the curved tube not only has an excellent pressure-bearing

capacity but also is easy to cast, is flexible and has potential for constructing a compact heat exchanger [45–47]. These advantages make curved tubes widely used in nuclear reactors, food processing, air conditioning, waste heat recovery, chemical engineering and aerospace industries. However, compared to a straight tube, a curved tube will induce a secondary flow motion, which makes flow and heat transfer more complex [16,19,29,48–52]. Based on a small ORC system with a capacity of 3 kW, Lazova et al. [53] experimentally studied the heat transfer characteristics of a supercritical R-404A in a helically coiled tube heat exchanger. The analysis of the matching relationship with the heat source showed that the real operating pinch point temperature difference of the heat exchanger was only 2 K (deviating from the design pinch point temperature difference by 10 K), mainly due to the fact that the correlation equation used for the calculation was obtained by correcting the correlation equation for supercritical fluids in a straight tube, which has a large error. Therefore, the flow and heat transfer characteristics of fluids at supercritical pressure flowing in a curved tube has been the focus of many researchers in recent years. The literature shows that heat transfer in curved tubes has two main features: instability of heat transfer and uneven circumferential heat transfer. Liu et al. [19,32] numerically studied the heat transfer instability of supercritical CO_2 heated in a helically coiled tube and found that unstable heat transfer conditions are more likely to lead to heat transfer deterioration. Sun et al. [54] studied the heat transfer and thermal oxidation of supercritical aviation kerosene in vertical U-tubes by using large-eddy simulations. The strong secondary flow driven by the centrifugal effect significantly enhances the heat transfer in the outside region and weakens the heat transfer in the inside region of a U-bend tube, resulting in circumferential wall temperature differences of up to 300 k in the present case. Similar, Wen et al.'s [55] experimental study showed that the outside heat transfer coefficient is on average 31.5% larger than that of the inside. Consequently, the total deposition amount at the outside of a U-bend tube is significantly higher than that on the inside, which will likely result in clogged cooling passages, valves and nozzles or even catastrophic aircraft failure.

To ensure the safety and stability of a curved-tube heat exchanger, accurate knowledge about the heat transfer characteristics of the supercritical fluids in the tube is essential to its design and optimization. Therefore, the authors present an exhaustive review of the available research works on the unique characteristics of supercritical fluids in curved tubes. Finally, the research gaps and outlooks that need to be considered for future studies are named.

2. Materials and Methods

2.1. Experimental Study

Figure 3 presents a schematic diagram of the experiment system constructed by Zhang et al. [49] for the measuring of the outer wall temperature in a vertically oriented helically coiled tube. The experimental facility is typical for most experimental studies on supercritical fluids. The test system consists of three parts: namely, the main system consists of a filling system, a temperature control system and a data-collecting system. Before working fluid charged, the main system was vacuumed to make sure the air and any non-condensable gases in the system were as minimal as possible. The mass flow rates are usually controlled by a high-pressure magnetic drive pump [31,52], while other studies have used a flow control valve and a bypass pipeline controlling the flow rates through the test section [16,49]. For the heating condition, the test section was heated by using electrical heating (with DC power, test section and system connected by insulating flange) [16,48,49], whereas the test section was cooled by tube-in-tube heat exchangers with water for cooling condition [31,52,56,57]. Armored K-type thermocouples were inserted into the inlet and outlet of the test section to measure the fluid temperature, and the total heat load of the test section was calculated based on the enthalpy difference between the inlet and outlet. For the heating condition, the heat flux was uniform, and the local fluid temperature along the test section was determined by the energy balance [16]. For the cooling condition, the local fluid temperature is hard to determine because of the non-uniform distribution along the

test section. Consequently, the test section was considered as a point and the wall and bulk temperature difference usually calculated with logarithm temperature difference between the inlet and outlet fluid temperature [31,56]. In order to obtain the wall temperature, a series of K-type thermocouples were welded onto the outer wall along the test section. For the heating condition, local wall temperature was the average value of all measurement points on a cross section. [49]. For the cooling condition, the outer wall temperature was the average value of all measurement points along the flow direction [31,52]. Then, the inner wall temperature based on Fourier's law of heat conduction could be calculated as shown in Equation (1):

$$T_{w,i} = T_{w,o} - \frac{Q}{2\pi\lambda l} \ln \frac{d_o}{d_i} \quad (1)$$

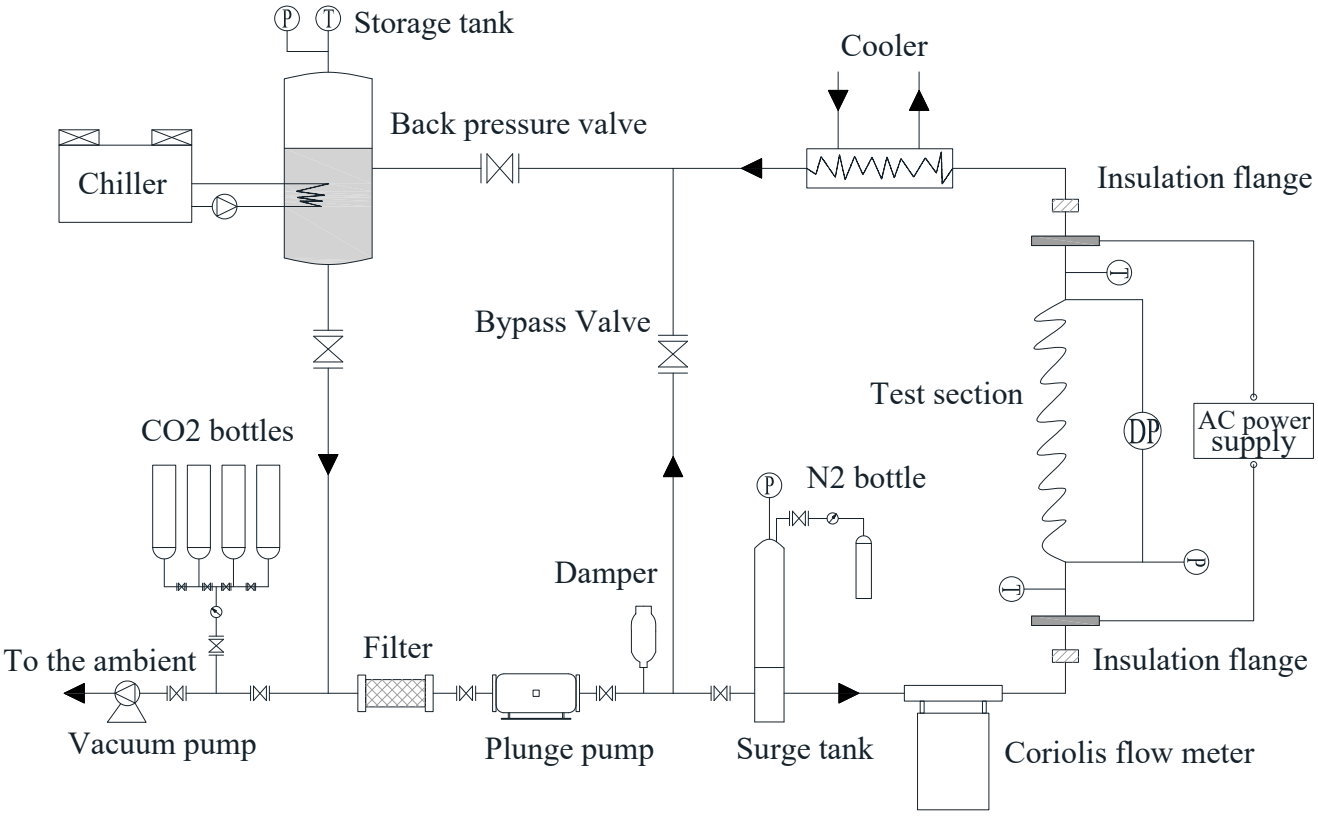

Figure 3. Schematic diagram of the experimental test facility for the investigation of the heat transfer of supercritical CO_2 in helically coiled tube [49].

The heat transfer coefficient was calculated with Equation (2).

$$h = \pm \frac{q}{(T_{w,i} - T_b)} \quad (2)$$

where the variables represent the heating and cooling conditions, respectively.

Due to the non-uniform distribution, the major difficulty in measuring the wall temperature of curved tubes is how to place enough thermocouples on the circumferential locations at the selected cross section. Therefore, the amount of experimental study on supercritical fluids flowing in curved tubes is relatively lower. Table 1 summarizes the available experimental studies' processes. In the future, more experimental studies could be conducted by using the infrared thermal imaging technique. Continuous wall temperatures can be obtained in both axial and circumferential directions [48,58]. It overcomes the deficiencies of scatter measurements with more precision and convenience. An example schematic diagram of experimental system for wall temperature measurement of

water flowing in helically coiled tube with infrared thermal imaging technique is shown in Figure 4.

Table 1. Summary of the available experimental studies on heat transfer characteristics of supercritical fluids in curved tubes.

Authors	Test Section Type	Principal Experimental Parameters	Flow Regime	Working Fluid
Zhang et al. [49]	Helically coiled tube	p = 8.02–10.05 MPa G = 0–650 kg·m^{-2}·s^{-1} q_w = 0.4–50 kW·m^{-2}	d_{in} = 9 mm, D = 12 mm, 2R = 283 mm, P = 32 mm, l = 5500 mm	CO_2
Xu et al. [59]	Serpentine tube	p = 8.0 MPa Re_{in} = 3200–5400 q_w = 9600–40700 W·m^{-2}	d_{in} = 0.953 mm, D = 8.01 mm, l= 88 mm	CO_2
Xu et al. [31]	Helically coiled tube	p = 7.5–9.0 MPa G = 79.6–238.7 kg·m^{-2}·s^{-1} T_b = 23–53 °C	d_{in} = 4 mm, D = 6 mm, 2R = 36 mm, P = 34 mm, l = 500 mm	CO_2
Xu et al. [60]	Helically coiled tube	p = 8.0 MPa G = 0–650 kg·m^{-2}·s^{-1} q_w = 0–50 kW·m^{-2}	d_{in} = 9 mm, D = 12 mm, 2R = 283 mm, P = 32 mm, l = 5500 mm	CO_2
Wang et al. [52]	Helically coiled tube	p = 8.0–9.0 MPa G = 159.0–318.2 kg·m^{-2}·s^{-1} q = 4200–24,300 W·m^{-2}	d_{in} = 4 mm, R = 36 mm, P = 34 mm, l = 560 mm	CO_2
Lazova et al. [53]	Helically coiled heat exchanger	p = 3.8–4.2 MPa m = 0.2–0.3 kg·s^{-1}	d_{in} = 25.7 mm, D = 33.7 mm, 2R = 600 mm, P = 42.1 mm, N = 35	R-404A
Fu et al. [16]	U-type tube	p = 3–5 MPa, G = 589–1375 kg·m^{-2}·s^{-1} q = 100–500 kW·m^{-2}, T_{in} = 400–523 K	d_{in} = 1.82 mm, D = 20/30/40 mm, l = 800 mm	Hydrocarbon fuel RP-3
Yang et al. [61]	Helix tube gas cooler	p = 8–10 MPa m = 0.2 kg·s^{-1} T_{in}= 373.15–393.15 K	d = 10 mm	CO_2
Xu et al. [57]	Helically coiled tube	p = 7.5–9.0 MPa G = 79.6–238.7 kg·m^{-2}·s^{-1} T_b = 23–53 °C	d_{in} = 2–4 mm, D = 6 mm, P = 34–80 mm, l = 500 mm	CO_2
Liu et al. [62]	Helically coiled tube	p = 7.5–9.0 MPa G = 79.6–238.7 kg·m^{-2}·s^{-1} T_b = 23–53 °C	d_{in} = 2–4 mm, D = 6 mm, P = 34–80 mm, l = 500 mm	CO_2
Wang et al. [63]	Helically coiled tube	p = 2–7.0 MPa, G = 100–1000 kg·m^{-2}·s^{-1} q= 75–450 kW·m^{-2},	d_{in}= 15.26 mm, D = 350 mm, 2R = 36 mm, P= 194 mm, l = 5100 mm	Water
Wang et al. [64]	S-bend tube	p = 4 MPa m = 1, 1.5, 2 g·s^{-1}	d= 2 mm, l = 1250 mm	Aviation kerosene RP-3
Lei et al. [65]	Helically coiled tube	p = 5 MPa m = 1–5 g·s^{-1}	d_{in} = 2–3 mm, D = 40–60 mm, P = 15 mm, δ = 0.05–0.075 mm, l = 1117 mm	RP-3
Han et al. [66]	Serpentine tube	p = 3–7 MPa m= 0.5–1.5 g·s^{-1} T_{in}= 290 K	d_{in}= 1 mm, D = 40 mm	RP-3 kerosene
Chang et al. [67]	Helically coiled tube	p = 24–28 MPa, G = 2500–4000 kg·m^{-2}·s^{-1} q= 210- 420 kW·m^{-2}	d_{in}= 8 mm, D = 650 mm, P= 181 mm, l= 2450 mm	Water
Liu et al. [68]	Helically coiled tube	p = 7.5–9 MPa, G = 120 kg·m^{-2}·s^{-1} q= 17.8–24.5 kW·m^{-2}	d = 9 mm, D = 283 mm, P = 32 mm, l = 5500 mm	CO_2
Zheng et al. [69]	Serpentine tube	p = 7.97–9.3 MPa Re_{in} = 190–660 q_w = 0.5–38.8 kW·m^{-2}	d_{in} = 0.953 mm, D = 8.01 mm, l= 88 mm	CO_2
Fu et al. [70]	Helically coiled tube	p = 5 MPa T_{in}= 400 K G = 393–1178 kg·m^{-2}·s^{-1}	d = 1.82 mm, D = 46–502 mm, P = 40 mm, l = 149.9–1500 mm	aviation kerosene RP-3
Wen et al. [55]	Helically coiled tube	p = 5 MPa T_{in}= 323–633 K G = 534.5–1572 kg·m^{-2}·s^{-1} q_w = 37–596 kW·m^{-2}	d = 1.82 mm, D = 20 mm, P = 10 mm, l = 1500 mm	aviation kerosene RP-3
Pei et al. [71]	S-bend tube	p = 3 MPa T_{in}= 300.15 K G = 534.5–1572 kg·m^{-2}·s^{-1} q_w = 115.3 kW·m^{-2}	d = 2 mm, l = 1500 mm	aviation kerosene RP-3

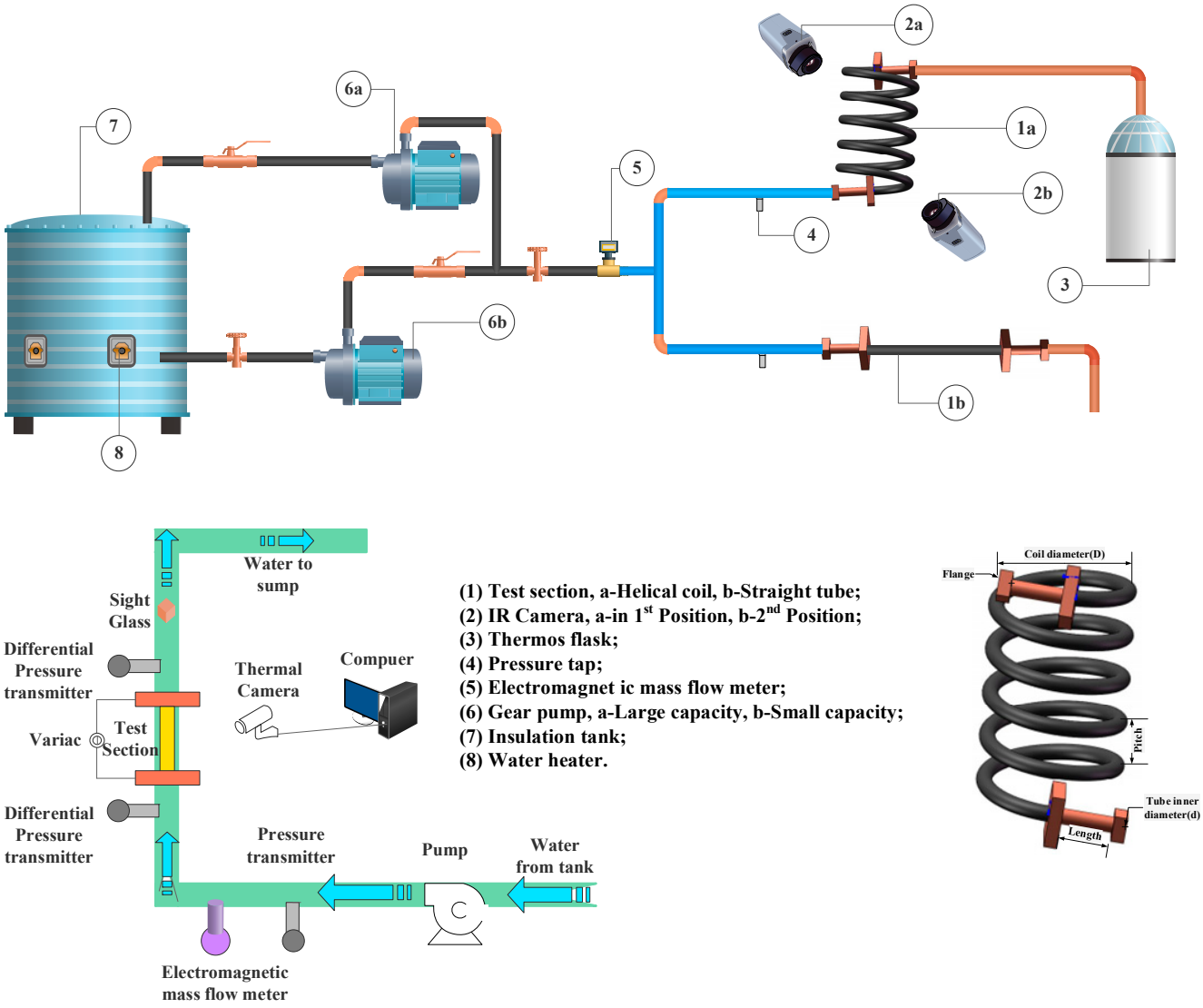

Figure 4. Schematic diagram of the experimental test rig with infrared thermal imaging technique [58].

2.2. Numerical Study

In recent years, with the significant development of computer processing power, numerical simulation has been proven as an efficient method to study flow and heat transfer in various channels, which can obtain the details of the flow that are difficult to observe by the experimental methods. What is more, numerical simulation can separate the buoyancy force from the centrifugal force in curved tubes, which is beneficial to obtaining insight into the individual mechanism of buoyancy or centrifugal force affecting the heat transfer performance.

Since there is no turbulent model specifically for supercritical fluid flow heat transfer, the existing supercritical fluid heat transfer simulations are mainly based on the RANS model. The governing equations can be described as follows:

Continuity:

$$\frac{\partial}{\partial x_j}(\rho u_j) = 0 \tag{3}$$

Momentum:

$$\partial(\rho u_j u_i)/\partial x_j = -\partial p/\partial x_i + \partial\left(\tau_{ij} - \rho u_i'' u_j''\right)/\partial x_j + \rho g_i \tag{4}$$

Energy:

$$\partial(\rho u_j h)/\partial x_j = \partial\left(\frac{\lambda}{c_p}\frac{\partial}{\partial x_j}h\right)/\partial x_j \quad (5)$$

where ρ, u and h are the density, velocity and enthalpy of the fluid, respectively. The viscous stress tensor τ_{ij} in Equation (4) is the additional unknown quantity arising from the time-averaged operation. Various types of turbulence models have emerged around how to represent the Reynolds stress in terms of known quantities so that the set of equations is closed.

The transport equations for the various RANS models can be expressed in a generic form.

$$\frac{\partial}{\partial x_i}\left[\rho k u_i - \left(\mu + \frac{\mu_t}{\sigma_k}\right)\frac{\partial k}{\partial x_i}\right] = P_k + G_k - \rho\varepsilon + \rho D \quad (6)$$

$$\frac{\partial}{\partial x_i}\left[\rho\varepsilon u_i - \left(\mu + \frac{\mu_t}{\sigma_\varepsilon}\right)\frac{\partial \varepsilon}{\partial x_i}\right] = (C_{\varepsilon 1} f_1 P_k + C_{\varepsilon 1} C_{\varepsilon 3} G_k - C_{\varepsilon 2} f_2 \rho\varepsilon)\frac{\varepsilon}{k} + \rho E \quad (7)$$

where

$$\mu_t = \frac{C_\mu f_\mu \rho \kappa^2}{\varepsilon} P_k = \mu_t\left(\frac{\partial u_i}{\partial x_j} + \frac{\partial u_j}{\partial x_i}\right)\frac{\partial u_i}{\partial x_j} G_k = \beta g_i \frac{\mu_t}{Pr_t}\frac{\partial T}{\partial x_i}; \beta = -\frac{1}{\rho}\frac{\partial \rho}{\partial T} \quad (8)$$

More information about the turbulence models can be found in the literature [72] or the Ansys help manual.

The flow and heat transfer characteristics of supercritical CO_2 in curved tubes have very strong three-dimensional phenomena. Therefore, the model and meshing cannot be symmetrically simplified [73,74], 1/4 simplified [3] or even two-dimensionalized [75–77] as they can be for straight pipes. Therefore, curved tubes require a large number of meshes, typically in the millions to tens of millions, to reach grid independence. This makes it necessary to configure higher-performance computers or workstations for related simulation studies.

Another important part of the numerical simulation is the model validation. Table 2 summarizes the available numerical studies on curved tubes under both cooling and heating processes. As shown in the table, most scholars validated their numerical methods by comparing the Nusselt number, heat transfer coefficient or wall temperature of the available experimental data in the literature [19,50,52,78,79]. However, due to the limited experimental and DNS database of supercritical fluids flowing in curved tubes, some studies can only validate the numerical calculations with experimental data in straight tubes [80] or empirical correlation with constant fluid properties [81,82]. Therefore, more experimental and DNS studies should be conducted to provide an abundant reliable database for numerical model validation.

ANSYS FLUENT is widely used for finite-volume numerical simulation. To effectively and accurately obtain the thermal physical properties distribution along the physical model, it is essential to choose an appropriate turbulence model. The turbulence model can be Spalart Allmaras (SA/RSM) [78], Renormalization Group (RNG) k-ε [30,60,61,81,83], RSM [80] or Shear Stress Transport SST *k*-ω [19,32,50,79,84]. As shown in Table 2, SST k-ω models and RNG *k*-ε model are mostly used in the previous numerical analysis. Wang et al. [72] discussed the applicability of nine turbulence models for the prediction of the experimental data with supercritical CO_2 heated in a vertical helically coiled tube under relatively low heat flux. They reported that the SST k-ω model yielded the optimal simulation result and the agreement between the experimental temperature and the predictions was good, with the largest difference being less than 10%. Differently from the former study, Xu et al. [60] conducted a similar numerical investigation of a helically coiled tube by using the RNG *k*-ε with enhanced wall treatment [85]. They point out that the RNG *k*-ε model added a correction item in the ε equation, which makes the model more accurate in dealing with flow in curvature pipes. Li et al. [82] simulated the super-

critical China No.3 aviation kerosene heated in a curved tube with two-layer turbulence model: the integrated model with RNG k-ϵ two-equation and Wolfstein one-equation. A constant value of gravity acceleration (10 m/s^2) and a source term Si were introduced in the governing equation to consider the buoyancy force and centrifugal force, respectively. Liang et al. [78] simulated the flow characteristics of the supercritical n-decane cooled in a square concave tube (a quarter of the circle). The parameters that characterize the flow fields calculated with Spalart–Allmaras and Reynolds stress models were compared. To improve the performance of PCHE, Cui et al. [86] comparatively studied the heat transfer performance of supercritical CO_2 in serpentine tubes with different cross-sectional shapes, and the results showed that among the many cross-sectional shapes, the circle-shape had the best heat transfer performance, and the vertical ellipse had the lowest flow friction. Fu et al. [70] numerically studied the thermal oxidation coking of supercritical aviation kerosene RP-3 heated in helically coiled tube. Their results confirmed that the maximum coking amount in a helically coiled tube is reduced by about 69.5% compared to a straight pipe under the same working conditions. Bai et al. investigated the icing process and thermal performance of the serpentine tube of a submerged combustion evaporator at supercritical pressure using SST *k*-*ω* and shell layer conduction model. A semi-empirical heat transfer relation equation as a function of thermal properties, secondary flow, flow acceleration and geometric factor was proposed based on the simulation data, which can accurately predict the heat transfer of LNG in the serpentine tube at supercritical pressure. From the above, it is clear that the existing numerical simulation studies are more concerned with the overall heat transfer performance. Less attention has been paid to the fluid structure inside the tube, the distribution of physical parameters, etc., but the authors believe that these are more important for the understanding of curved-tube heat transfer and the optimization of the tube structure.

Although the RANS model can qualitatively predict the complex heat transfer behavior of turbulent flows under supercritical conditions, there are still significant deviations in the quantiles near the pseudo-critical temperature [32,87]. Studies of supercritical fluids in straight tubes show that LES [3,14] and DNS [88–90] have high accuracy in numerical simulations. However, it can be seen from Table 2 that LES and DNS almost form a gap in the study of supercritical fluids in curved tubes. Further research is needed to discover a more accurate prediction model that can adequately take into account various factors such as drastic physical property changes, buoyancy and curvature effects.

Table 2. Summary of the available numerical studies on supercritical fluids in curved tubes.

Author	Section Type	Boundary Condition	Flow Regime	Working Fluid	Turbulent Model	Validation
Li et al. [81]	Curved pipe	Constant wall temperature	δ = 0.05, N = 1	H_2O	RNG *k*-*ε*	Compare *Nu*
Zhao et al. [29]	Helically coiled tube	Constant wall heat flux	d = 7.5 mm, D = 200, 400 mm, b = 8 mm, l = 2281 mm	H_2O	SST *k*-*ω*	Compare *h*
Xu et al. [60]	Helically coiled tube	Constant wall heat flux	d = 9 mm, 2R = 283 mm, b = 32 mm, l = 5500 mm	CO_2	RNG *k*-*ε*	Compare T_w
Yang [30,83]	Helically coiled tube	Constant wall heat flux	d = 4 mm, D = 40 mm, b = 10 mm, l = 2000 mm	CO_2	RNG *k*-*ε*	Compare *h*
Li et al. [79]	Helically coiled tube	Coupled boundary condition	d = 9 mm, D = 283 mm, b = 32 mm, l = 5500 mm	CO_2	SST *k*-*ω*	Compare *h* and T_w
Liu et al. [19]	Helically coiled tube	Constant wall heat flux	d = 9 mm, D = 283 mm, P = 32 mm, l = 5500 mm	CO_2	SST *k*-*ω*	Compare *h*, T_w and T_b
Zhao et al. [91]	Helically coiled tube	Coupled boundary condition	d = 6 mm, D = 80 mm, b = 12 mm, N = 10	CO_2	AKN *k*-*ε*	Compare *h*
Zhang et al. [92]	Helically coiled tube	Constant wall heat flux	d = 9 mm, D = 283 mm, P = 32 mm, l = 5500 mm	CO_2	SST *k*-*ω*	Compare *K*
Ciofalo et al. [93]	Toroidal pipe and helically coiled pipe	Wall temperature linearly increasing along flow direction	d = 0.9, λ = 0.4	–	–	–
Wang et al. [80]		Constant wall temperature	d = 20 mm, D = 300 mm, b = 30 mm, N = 11	Methane	RSM	Compare *h*

Table 2. *Cont.*

Author	Section Type	Boundary Condition	Flow Regime	Working Fluid	Turbulent Model	Validation
Liang et al. [78]	Concave, heated, 90° bend	Coupled boundary condition	square tube, hydraulic diameter d = 2 mm, D = 100 mm	n-Decane	–	Compare Nu
Yang et al. [61]	Helix tube gas cooler	Coupled boundary condition	d = 10 mm	CO_2	k-ω	–
Li et al. [82]	Curved tubes	The true distribution of heat flux of scramjet	d = 12 mm, D = 300 mm, l = 4500 mm	China No.3 aviation kerosene	*RNG* k-ϵ	Compare Nu
Liu et al. [32]	Helically coiled tube	Constant wall heat flux	d = 4–16 mm, D = 150–283 mm, l = 5500 mm, N = 5	CO_2	SST k-ω	Compare h and T
Zhang et al. [92]	Helically coiled tube	Constant wall heat flux	d = 9 mm, D = 283 mm, P = 32 mm, l = 5500 mm	CO_2	SST k-ω	Compare h
Yi et al. [94]	Serpentine micro-tube	Constant wall heat flux	d = 1 mm, D = 8 mm, l = 7Rπ mm	CO_2	RNG k-ε	Compare T_w
Sun et al. [54]	U-tube	Constant wall heat flux	d = 1.82 mm, D = 30 mm,	Aviation kerosene	LES	Compare T_w
Li et al. [95]	Helically coiled channels	One-side heating with Constant wall heat flux	d = 9 mm, D = 283 mm, b = 32 mm, l = 5500 mm	CO_2	SST k-ω	Compare h and T_w
Jiang et al. [96,97]	Helically coiled tube	Constant wall heat flux	d = 12 mm, D = 70 mm, b = 32 mm, l = 1222 mm	s-R1234ze€	SST k-ω	Compare h
Huang et al. [98]	U-tubes	Constant wall heat flux	d = 1.82 mm, D= 40 mm	CO_2	Standard k-ε	Compare T_w
Luo et al. [99]	Helically coiled heat exchangers	Convective heat transfer	d = 3 mm, D = 40 mm, P = 15 mm	Air and n-decane	RNG k-ε	Compare Nu
Bai et al. [100]	Serpentine tube	Constant wall heat flux	d = 15 mm, D = 100 mm	LNG	SST k-ω	Compare T_w
Zhang et al. [101]	Helically coiled tube	Constant wall heat flux	d = 9 mm, 2R = 150–283 mm, b = 32 mm, l = 5500 mm	CO_2	SST k-ω	Compare T_w and T_b
Cui et al. [86]	Serpentine channel	Constant wall heat flux	d = 1.8 mm, D = 3.62 mm	CO_2	SST k-ω	Compare h
Li et al. [102]	Helically coiled tube	One-side heating with Constant wall heat flux	d = 9 mm, 2R = 283 mm, b = 32 mm, l = 5340 mm	Water	RNG k-ε	Compare T_w and T_b

3. Heat Transfer Characteristics of Supercritical Fluid in Curved Tubes

As is known by all, the heat transfer efficiency in curved tubes is higher compared to straight tubes due to the secondary flow inducted by the curvature effect. Xu et al. [31] gave a comparison of the heat transfer performance between a helically coiled tube and a straight tube. The comparison shows that the helically coiled tube can enhance the heat transfer coefficients by up to about 15% compared to straight tube. Similar, Xu et al. [48] pointed out that a serpentine tube can increase the heat transfer efficiency due to the centrifugal forces. What is more, the unfavorable heat transfer deterioration was suppressed. Liu et al. [32] also confirmed that a helically coiled tube can delay heat transfer deterioration, especially when the helically coiled tube is vertically positioned.

Most previous studies have shown that centrifugal force coupled with buoyancy force can effectively increase the heat transfer efficiency of curved tubes. Centrifugal force caused by the curvature is closely related to tube diameter and coil diameter. Dean [103] proposed a single non-dimensional Dean number to take into account the centrifugal force effect on the flow in the curved tubes. This parameter was defined as $De = Re\sqrt{\delta}$, where Re is the Reynolds number and $\delta = a/R$ is the curvature ratio. Li et al. [79] numerically studied the helical tube structure parameter effect on the heat transfer performance. Results showed that the flow accompanied by the strong secondary flow caused by the curvature can significantly suppress the buoyancy effect. Chen et al. [104] numerically studied the tube structure parameter and the tube orientation effects on the flow characteristics of supercritical CO_2 heated in U-ducts. Results show that the U-ducts' structure mainly affects the temperature fields distribution after the turn due to the flow separation and reattachment. Fu et al. [16] studied the flow characteristics of supercritical RP-3 heated in U-turn tubes with various bending diameters. The results show that with the bending diameter decreasing from 40 to 20 mm, the heat transfer coefficient can be increased by more than 40% to 2 compared that in a straight tube. Despite numerous studies having

been conducted on the effects of tube and coil diameter, the explicit relationship between these effects and heat transfer performance has not been established, and there is a lack of universal heat transfer correlation that contains the geometry factor.

It was accepted that the flow characteristics of fluids at supercritical pressure are mainly affected by thermos-physical properties, boundary condition, flow direction and tube structure. The aforementioned parameters of flow characteristics in a straight tube have been widely studied and reviewed in the open literature [6,9,105–109]. However, the boundary condition effects are related to the thermal-physical properties distribution in the cross section and have no effect on the flow structure. Consequently, their effects on the flow characteristics in curved tubes are mostly the same as in straight tubes, so these will not be covered again. However, differently from a straight tube, a curved tube would lead to two horizontal vortices, which has a significant impact on the flow structure and makes the heat transfer behavior more complicated (as shown in Figure 5a). As is well known, in a straight tube, the tube orientation influence on the heat transfer performance is actually the buoyancy force [59,110–116]. In the curved tubes, centrifugal force is always perpendicular to the flow direction and has the same effects on the flow structure at different tube orientations. Hence, buoyancy force is also the key factor in the abnormal heat transfer phenomenon with different flow direction and tube orientation [19,48,104]. Due to non-coplanar flow direction and buoyancy force, the gravitational buoyancy can be decomposed into two parts in curved tubes: the first component projected onto radial direction (mainly affecting the circumferential heat transfer distribution) and the second component parallel to the axial direction (mainly affecting the average heat transfer distribution). Therefore, the following discussion on the flow direction is divided into two parts.

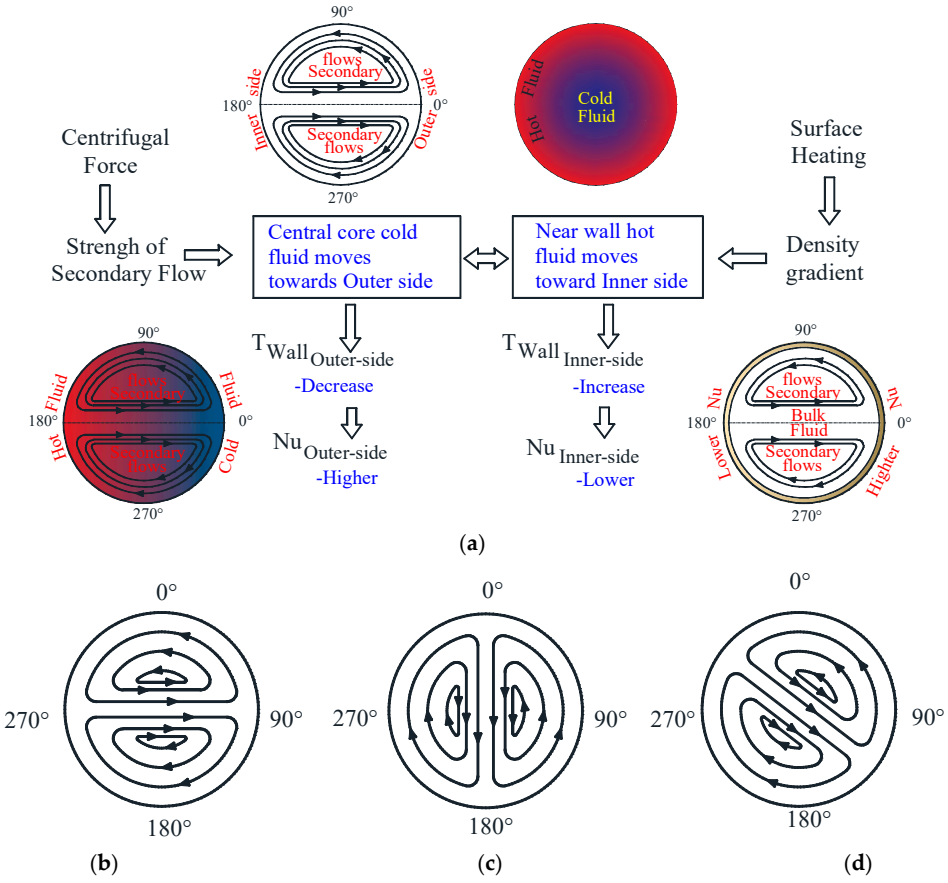

Figure 5. (**a**) Phenomenal chart for wall temperature and Nusselt number distribution caused by centrifugal force [58]; Schematic of secondary cross-section flow structures [49] caused by (**b**) only centrifugal force; (**c**) only buoyancy force; (**d**) combination effects of centrifugal and buoyancy force [49].

3.1. The Effect of Buoyancy Force on Circumferential Distribution

As mentioned above, the centrifugal force is always perpendicular to the axial and will cause the non-uniformity of the flow structure. Therefore, the non-uniformity heat transfer coefficients of a cross section are affected by the combined first component buoyancy force and centrifugal force [16,19,49,93,117]. Figure 5b,c provides the schematic diagram of the secondary flow structures caused by individual centrifugal force and individual buoyancy force at a selected cross section in the vertical helically coiled tube. The individual centrifugal force causes the highest bulk temperature region, located at the inner side of the cross section, and the individual buoyancy force causes the highest bulk temperature, located at the upside of the cross section. Hence, under the combined effect of buoyancy force and centrifugal force, the position of the highest bulk temperature deflect and the location will depend on the relative value of the two forces. Xu et al. [49,60] experimentally investigated the non-uniform wall temperature distribution direction in a vertical orientated helically coiled tube by welding eight equally spaced thermocouples at the selected cross section. The wall temperatures vary parabolically along the circumference direction, and the highest wall temperature is located at about $\phi = 135^{\circ}$. Similar conclusions are reported in the study [32]. Liu et al. [19] simulated the non-uniformity of wall temperature distribution in a helically coiled tube at various inclination angles. The results show that in a vertical helically coiled tube, the position relationship and coupled angle between buoyancy force and the centrifugal force remain constant at each cross section (Figure 5d). However, in an inclined helically coiled tube, the position relationship and coupled angle between them changes periodically along the flow direction, reinforcing each other's effects on the heat transfer at the lower half of the curved tubes and weakening their respective effects on the heat transfer at the upper half of the curved tubes. In addition, Liu et al. [32] point out that the non-uniformity of wall temperature can be suppressed by increasing the wall thickness. Meanwhile, some studies assume the tube wall thickness to be zero in the strong three-dimensional geometries or the horizontal simplified 2D model (straight tube). This would cause a larger error in the simulation of circumferential wall temperature.

To quantify the importance of the centrifugal force and buoyancy force acting on a selected cross section, some researchers have proposed corresponding non-dimensional parameters based on their theoretical analysis (list in Table 3). Ciofalo et al. [93] suggested that the flow in curved tubes is affected by two kinds of buoyancy effects. One is the traditional gravitational buoyancy force, defined as

$$Ri_g = \frac{Gr_g}{Re^2} = -g_z \frac{\rho_b - \rho_w}{\rho_b} \frac{a}{4U^2} \tag{9}$$

The other is the centrifugal buoyancy force induced by centrifugal force:

$$Ri_c = \frac{Gr_c}{Re^2} = \frac{\delta}{4} \frac{\rho_b - \rho_w}{\rho_b} \tag{10}$$

The ratio ϕ is introduced to quantify the importance of the two types of buoyancy, and $\phi = 1$ means that two kinds of buoyancy effects exhibited the same order.

$$\phi = \frac{Ri_c}{Ri_g} = \frac{\delta \nu_b^2}{4a^3 g_z} Re^2 \tag{11}$$

Li et al. [79] point out the centrifugal buoyancy parameters (Equation (5)) only present the second-order buoyancy effect, which is caused by the variable physical properties. However, as for centrifugal force, its first-order effect (u^2/r) can also cause the non-uniformity of the cross-section flow structure. Hence, Li et al. [79] modified Ciofalo's parameter by considering the first-order effect of the centrifugal force:

$$Ri_c = ri_{c,1st} + R_{ic,2} = \frac{Gr_c}{Re_b^2} \tag{12}$$

where

$$Gr_c = Gr_{c,1st} + Gr_{c,2nd} = 2\delta\frac{2\rho_b - \rho_w}{\rho_b}\mathrm{Re}_b^2 \quad (13)$$

The ratio of the two forces can be expressed as:

$$\phi = \frac{Ri_c}{Ri_g} = \frac{\delta\nu_b^2}{4a^3 g_z}\mathrm{Re}^2 \quad (14)$$

Zhang et al. [92] modified the Dean number by considering the effect of coiled pitch and proposed a similar parameter based on the new Dean number. Wang et al. [63] experimentally studied the circumferential wall temperature distribution in a helically coiled pipe with water at constant pressure. A similar non-dimensional parameter to manifest the relative importance of centrifugal force and buoyancy force was proposed. However, details on the process of developing the parameter were not listed in the paper.

Table 3. Summary of the proposed dimensionless parameter to determine the relative strength of buoyancy force and centrifugal force.

Author	Working Fluid	Parameter	Threshold
Ciofalo et al. [93]	Author defined	$\phi = \frac{Ri_c}{Ri_g} = -\frac{\delta\nu_b^2}{4a^3 g_z}\mathrm{Re}^2$, where $Ri_c = \frac{Gr_c}{\mathrm{Re}^2} = \frac{\delta}{4}\frac{\rho_b - \rho_w}{\rho_b}$ and $Ri_g = \frac{Gr_g}{\mathrm{Re}^2} = -g_z\frac{\rho_b - \rho_w}{\rho_b}\frac{a}{4U^2}$	$g_z < 0$, $T_w - T_b > 0$ yield $Ri_g > 0$, $Ri_c > 0$ (positive gravitational and centrifugal buoyancy); $g_z > 0$, $T_w - T_b > 0$ yield $Ri_g < 0$, $Ri_c > 0$ (negative gravitational, positive centrifugal buoyancy). $g_z > 0$, $T_w - T_b < 0$ yield $Ri_g < 0$, $Ri_c < 0$ (positive gravitational, negative centrifugal buoyancy); $g_z < 0$, $T_w - T_b < 0$ yield $Ri_g > 0$, $Ri_c < 0$ (negative gravitational and centrifugal buoyancy).
Wang et al. [63]	Constant water	$Lu = \frac{\frac{V^2}{D}\rho bd}{\rho_b\beta_b(T_w - T_b)dg} = \frac{V^2}{D\beta_b(T_w - T_b)g}$	When $Lu < 0.25$, the heat transfer coefficient divided into two regions and the maximum heat transfer coefficient appears at the bottom of helical coil tube. When $0.25 < Lu < 0.5$, the heat transfer coefficient at location B and F is much lower than region I and much higher than region III. When $Lu > 1.5$, the heat transfer intensity could be divided into three regions.
Li et al. [79]	Supercritical CO_2	$\phi = \frac{Ri_c}{Ri_g} = \frac{\delta\nu_b^2}{4a^3 g_z}\mathrm{Re}^2$, where $Ri_c = ri_{c,1st} + R_{ic,2} = \frac{Gr_c}{\mathrm{Re}_b^2}$, $Gr_c = Gr_{c,1st} + Gr_{c,2nd} = 2\delta\frac{2\rho_b - \rho_w}{\rho_b}\mathrm{Re}_b^2$	Similar to Ciofalo's
Zhang et al. [92]	Supercritical CO_2	$\phi^2 = \left(\frac{\overline{u}_{Gr}}{\overline{u}_{De}}\right)^2 = \frac{Gr}{2De*^2}$	Inclined angle estimated by non-dimension buoyancy parameter φ^2 ($\tan\alpha \approx \phi$). The inclination angle α is equal to 45° when $\phi \approx 1$, which demonstrates that the buoyancy and centrifugal force have an equivalent diameter. The centrifugal force dominates heat transfer when $\alpha < 45°$, and the buoyancy force dominates heat transfer at the $\alpha > 45°$.

3.2. The Effect of Flow Direction on the Axial Direction

In the curved tubes, the flow direction constantly changes along the flow direction which coupled with the centrifugal force makes the flow mechanism more complex. Therefore, the effect of flow direction on the flow characteristics in curved tubes were widely investigated to obtain insight into the coupled effects of the buoyancy force and centrifugal force. Chen et al. [104] numerically studied the heat transfer coefficient of CO_2 at supercritical pressure flowing in U-ducts and confirmed that the average heat transfer coefficient in vertical downward U-ducts is higher than the horizontal and vertical upward ones because of the buoyancy force being opposite to flow direction. Li et al. [50] numerically compared the orientation effect on heat transfer with helically coiled tubes positioned horizontally and vertically. The results show that the overall heat transfer coefficient of the horizontal helically coiled tube was higher than that in the vertical one. In addition, the heat transfer coefficient in the downward flow direction was slightly higher than the upward flow direction. Liu et al. [19] also studied the orientation effects on the heat transfer

of supercritical CO_2 in a helically coiled tube. The results showed that the heat transfer coefficient experienced oscillation with the decreasing of the inclination angles and the maximum amplitude occurred in horizontal helically coiled tube (Figure 6). Consequently, the heat transfer deterioration most likely occurred in a horizontal helically coiled tube [32]. The oscillation phenomenon was also obtained in Xu et al. [48] experimental study on the vertical serpentine tube. As can be seen from Figure 7, the blue arrow represents the direction of flow and the red arrow represents the buoyancy force. The oscillation is mainly caused by the fact that the angles between the flow direction and buoyancy force periodic variation along the axial, whether it is upward or downward flow.

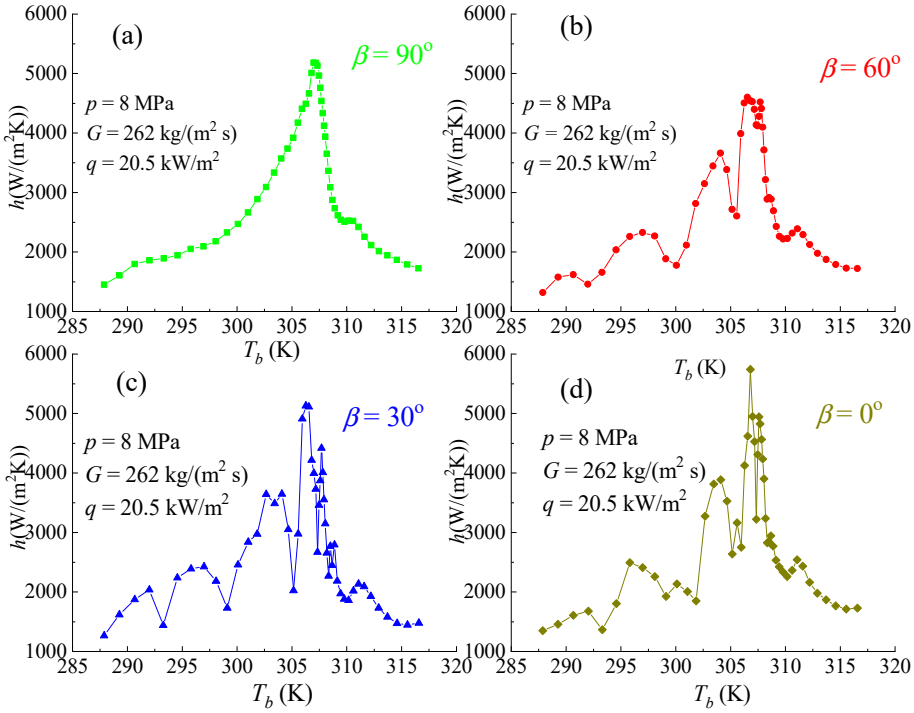

Figure 6. The heat transfer coefficient of supercritical CO_2 flowing in helically coiled tube at various dip angles [19]: (**a**) vertical without oscillation (β = 90°); (**b**) incline with small oscillation (β = 60°); (**c**) incline with mild oscillation (β = 30°); (**d**) horizontal with severe oscillation (β = 0°).

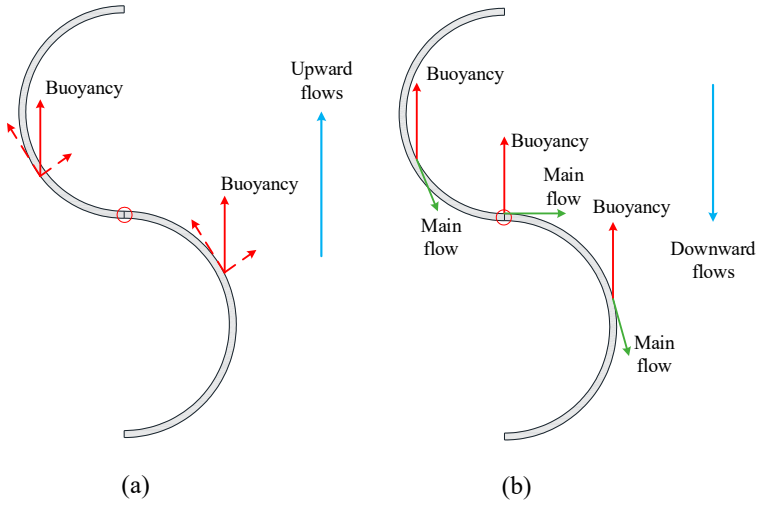

Figure 7. Schematic diagram of buoyancy effect on fluid flow in vertical serpentine tube [30]. (**a**) Upward flows (the buoyancy force or its component in the same direction as the main flow); (**b**) downward flows (the buoyancy force or its component in the opposite direction of the main flow).

The mechanism of the buoyancy force affecting the flow characteristics is always the focus of the study of supercritical fluids. Based on experimental measurement, numerical data and theoretical analysis, several buoyancy criteria have been proposed to evaluate its effects on the heat transfer performance in straight tubes. Recently, a comprehensive review on the existing buoyancy criteria was performed by Huang et al. [105]. For the vertical condition, the non-dimensional parameter $Gr/Re^{2.7}$ proposed by Jackson and Hall [110] is more accurate. For the horizontal condition, the non-dimensional parameter $Gr_q = Gr_{th}$ proposed by Petukhov et al. [118] is more accurate. As discussed in the previous literature review, the buoyancy force is still significant in its effect on the flow characteristics despite the centrifugal force being able to suppress its effect to some extent. Recently, many studies have been carried out to study the mechanism of buoyancy effects in curved tubes. Most of the studies show that the buoyancy force criterion for predicting buoyancy force effects in straight tubes are not suitable for curved tubes.

Fu et al. [16] analyzed the parameter $Gr_q = Gr_{th}$ and confirmed that the onset value $Gr_q = Gr_{th} > 2$ can effectively evaluate the buoyancy force in U-turn tubes. Wang et al. [52] used three buoyancy parameters, Bu_p, Gr_{th}/Gr_q and Ri, to evaluate the buoyancy force effect on the heat transfer of supercritical CO_2 cooled helically coiled tubes. Through the comparing of heat transfer coefficients in vertical and horizontal helically coiled tubes, they confirmed that the buoyancy force plays a major role in the gas-like region ($T_b > T_{pc}$), which is different, from the heating condition where the buoyancy force is significant in the liquid-like region. Furthermore, the results showed that all the three parameters overestimated the buoyancy force.

Wang et al. [80] pointed out that both the Gr/Re^2 and $Gr/Re^{2.7}$ parameters can effectively predict the buoyancy force in a helically coiled tube based on their numerical study of supercritical methane. However, Xu's [72] study of supercritical CO_2 indicated that the parameter of $Gr/Re^{2.7}$ was incapable of predicting the influence of buoyancy force in a vertical helically coiled tube.

Li et al. [50] evaluated the parameter Bo^* in the helically coiled tube with various tube geometries (with coils' dimensionless curvature δ ranging from 0.01 to 0.1), and the result showed that the buoyancy force effect can be ignored when the $Bo^* < 10^{-5}$. In a similar experimental study on a vertical helically coiled tube, Zhang et al. [49] confirmed that the buoyancy force can be ignored when $Bo^* \leq 4 \times 10^{-8}$, as the forced convection dominates the heat transfer. With the same buoyancy force criterion, the onset value of buoyancy can differ by orders of magnitude. Xu et al. [48] made measurements of the heat transfer distribution in a serpentine tube. Results showed the buoyancy force can intensify the heat transfer in the downward flow at $1.2 \times 10^{-7} < Bo^* < 5.6 \times 10^{-7}$ and the heat transfer coefficient is higher in the downward flow compared to the upward flow. However, within the Bo^* range from 5.6×10^{-7} to 5×10^{-6}, the heat transfer in the upward flow performed better than downward flow, which is contrary to the accepted conclusion obtained in straight tubes.

From what has been discussed above, it can be found that the buoyancy force's effect on the flow characteristics in curved tubes cannot be properly predicted by a buoyancy criterion derived from theoretical analysis based on straight tubes. The reasons may be the non-uniform distribution of the boundary layer caused by the combined effect of buoyancy force and centrifugal force and the inappropriate assumptions derived from the straight tube. Hence, Liu et al. [32] modified the buoyancy force criterion by considering the integrated centrifugal force and gravitational force and using the Dn number instead of the Re to consider the inertia force in the helically coiled tube. The modified buoyancy criterion is defined as:

$$Ri_{HCT} = \frac{Gr_{HCT}}{Dn^{2.7}} = -\sqrt{g^2 + \left(\frac{U^2}{d/2}\right)^2} \frac{\rho_b - \rho_w}{\rho_b} \frac{a^3}{\nu_b^2} \frac{2d}{4U} \quad (15)$$

Liu et al. [62] also introduced a new criterion to elevate the onset of buoyancy force in horizontal helically coiled tubes based on the theory of reduction of shear stress. The new parameter considered the curvature effect is defined as:

$$\frac{\Delta\tau_{bu}}{\tau_w} = \frac{\overline{Gr_b}}{Re^{2.7}Pr_b^{0.4}\delta^{0.15}}\left(\frac{\mu_w}{\mu_b}\right)\left(\frac{\rho_b}{\rho_w}\right)^{0.5} \quad (16)$$

Similarly, to predict the heat transfer coefficient of supercritical fluids in curved tubes, correlations of Yi et al. [94], Lei et al. [65], Huang et al. [98], Bai et al. [100], Zhang et al. [92], Wen et al. [55], Pei et al. [71] and Zhang et al. [49] have been proposed. All of these correlations for curved tubes are based on the heat transfer correlation for straight tubes. These correlations take into account the complex physical changes in supercritical fluids and curved-tube structure parameters and are successful in predicting the accuracy of their own experimental and simulation data results. However, due to the complexity of the curved-tube structure, the focus of each study is different, resulting in the correlations not being universal and accurate in form and prediction of results for others. Therefore, a large number of related studies need to be further developed and unified.

4. Future Work and Prospect

The aforementioned literature shows that curved tubes have certain advantages over straight tubes in enhancing heat transfer of supercritical fluids. However, the complexity of the tube structure brings new challenges to supercritical fluid in curved tubes. It is clear that the research methods for the study of supercritical fluids in curved tubes are the same as those in straight tubes, i.e., experiments and numerical simulations. However, the three-dimensional heat transfer characteristics in curved tubes give rise to the inapplicability of the scattered-point measurement method commonly used in straight tubes. A large number of test points are required to obtain the temperature distribution over a certain cross section, making it difficult to obtain the temperature distribution over the whole tube. Therefore, more experimental studies should be conducted by using infrared thermal imaging technique to provide an abundant database in the future. Compared with experimental studies, more researchers investigated the heat transfer characteristics of supercritical fluids by using numerical simulation. Numerical simulations not only are more economically efficient than experimental studies but also provide detailed flow field information that cannot be observed by experimental methods. However, there is no fully reliable turbulence model (RANS) that covers all phenomena of supercritical fluid flow and predicts the wall temperature accurately in all cases. Further studies are needed to construct more accurate prediction models. In addition, the LES and DNS models need to be given sufficient attention in the study of supercritical fluids in curved tubes.

The study of supercritical fluids in curved tubes is in its infancy, and the effects of some key factors on the heat transfer performance are still undiscovered. In terms of research content, the selection of various heat transfer parameters is only representative, and more experimental and computational simulation studies can be carried out in the future with a wider range of parameters. In addition, as the basic element of heat exchangers, the actual engineering conditions are dominated by the convective heat transfer boundary condition. However, the literature shows that the current research is mainly in constant heat flow flux or constant wall temperature. Subsequent studies need to pay more attention to convective heat transfer or the non-uniform heating boundary condition. In terms of heat transfer mechanisms, the results of studies in straight tubes have shown that the microscopic evolution of the boundary layer is important for revealing macroscopic heat transfer phenomena. However, current studies on the heat transfer of supercritical fluids in curved tubes have neglected this aspect. More importantly, an in-depth understanding of the boundary layer can provide theoretical guidance for studies on improving the heat transfer performance of curved tubes using roughness, which needs to be supplemented.

Differing from straight tubes, the effects of the buoyancy force in curved tubes are closely related to the centrifugal force because of the larger density differences at a cross

section. Hence, the mechanism of integrated buoyancy force and centrifugal force affecting both the circumferential and average heat transfer in curved tubes needs further study. On the other hand, the buoyancy force in curved tubes cannot be properly predicted by buoyancy criterion derived from straight tubes, and new empirical criterion should be proposed. In addition, due to the complexity of the curved tube structure, the focus of each study is different, resulting in the correlations not being universal and accurate in form and prediction of results for others. Therefore, a heat transfer correlation for supercritical fluids in curved tubes with general applicability needs to be developed.

As discussed in the Introduction, the existing enhanced heat transfer measures can be divided into two categories: one is to change the roughness of the tube wall, such as internal ribbed tubes, internal threaded tubes and foam metal tubes; the other is to change the structure of the tube, such as helically coiled tubes, serpentine tubes and U-shaped tubes. The literature shows that although changing the structure of the tube strengthens the heat exchange to a certain extent, it also causes two undesired features: instability of heat transfer and non-uniform circumferential heat transfer. Therefore, coupling the above two strengthening methods, elimination or suppression of two undesired phenomena in the curved tube by wall roughness needs sufficient attention.

5. Conclusions

Supercritical fluids are widely used in energy systems because of their excellent thermal properties. However, due to their physical properties, the heat transfer process is different from that of conventional fluids. One of the most important concerns is the suppression of heat transfer deterioration. To suppress heat transfer deterioration and improve heat exchanger performance, extensive attention has been paid to the supercritical fluids in curved tubes. In this paper, the studies in recent years are summarized and analyzed to provide a scientific basis for subsequent research and the design and optimization of curved-tube heat exchangers. The main conclusions are as follows:

1. Experimental and simulation studies show that the effect of working conditions on the heat transfer of supercritical fluid flow in curved tubes is basically the same as that in straight tubes: as the mass flow rate decreases, the pressure and heat flow density increase and the heat transfer coefficient decreases.
2. The experimental study provides basic data for the quantitative concept and simulation validation of supercritical fluids in curved tubes. However, the significant three-dimensional characteristics make the popular scattered-point measurement method deficient in obtaining the overall heat transfer performance of supercritical fluids in curved tubes. In the future, advanced thermal imaging technologies should be intentionally applied in this field.
3. By analyzing the cross-sectional vortex vector diagram, temperature, velocity and turbulent kinetic energy cloud diagrams, scholars concluded that the curved-tube circumferential heat transfer is influenced by centrifugal force, centrifugal buoyancy force, and gravitational buoyancy force. According to their theoretical analyses, a criterion for determining the relative magnitude of the buoyancy force and centrifugal force is developed. However, most simulation studies focus on the overall performance of curved tubes, ignoring the absolute advantage of simulation in gaining insight into the physical properties' distribution and the flow structure in the boundary layer of the fluid.
4. There is no consensus on the heat transfer correlation of supercritical fluids in curved tubes. On the one hand, it is because the criteria for determining the buoyancy force in curved tubes are uncertain; on the other hand, it is because the structure of curved tubes is more complicated than that of straight tubes, and the form of the structural parameters in the correlations is not yet settled.
5. Curved tubes can enhance heat transfer and suppress deterioration effectively. However, the heat transfer in curved tubes has two undesired features: instability of heat transfer and uneven circumferential heat transfer. To suppress the above two features,

the coupling of curved tubes and rough elements to enhance supercritical fluid heat transfer will be a hot spot for future research.

Author Contributions: Conceptualization, writing—original draft preparation, X.L. and S.L.; methodology, project administration, L.L. and C.H.; formal analysis, Z.S. and F.Ö.; writing—review and editing, M.A. and P.-C.K. All authors have read and agreed to the published version of the manuscript.

Funding: Liu Xinxin gratefully acknowledge the supports provided by the Natural Science Foundation of Henan Province (No. 212300410162), Natural Science Youth Innovation Fund of Henan Agricultural University (No. KJCX2021A11). The authors also acknowledge the financial support of Ministry of National Education, Turkey and Japan Society for the Promotion of Science under Grant No. JP-22F21041.

Data Availability Statement: The data presented in this study are available in this article.

Conflicts of Interest: The authors declare no conflict of interest.

Nomenclature

b	coil pitch divided by 2π [mm]
Bo*	non-dimensional buoyancy force $Bo^* = Gr^*/Re_b^{3.425}Pr_b^{0.8}$
Bu	non-dimensional buoyancy force $Bu = \overline{Gr_b}/Re_b^{2.7}$
c_p	specific heat (J/kg·K)
d	tube diameter [mm]
D	curvature diameter [mm]
Dn	Dean number
g	gravitational acceleration (m/s^2)
G	mass flux [kg/(m^2·s)]
Gr*	Grashof number $Gr^* = \frac{\rho_b(\rho_b-\rho_w)qgd^4}{\mu_b^2(t_w-t_b)\lambda_b}$
$\overline{Gr}$	Grashof number $Gr^* = \frac{\rho_b(\rho_b-\rho_w)qgd^4}{\mu_b^2(t_w-t_b)\lambda_b}$
h	heat transfer coefficient [W/(m^2·K)]
l	length of tube [mm]
m	mass flow rate [kg/s]
Nu	Nusselt numbers
p	pressure [MPa]
q	heat flux [W/m^2]
Re	Reynolds number
Ri	Richardson number
Si	$S_i = \rho\frac{W^2}{R+dR}$
T	temperature [K]
$\overline{T}$	average temperature [K]
u	velocity [m/s]
Greek symbols	
δ	curvature ratio [a/D]
α	global azimuthal angle around the curvature axis [°]
λ	thermal conductivity [W/(m·K)]
β	dip angle [°]
μ	dynamic viscosity [Pa/s]
ρ	density [kg/m^3]
Subscripts	
b	bulk fluid
i	inlet
HCT	helically coiled tube
o	outlet
w	wall

Abbreviations

DNS	direct numerical simulation
LES	large-eddy simulation
PC	pseudo-critical temperature
RANS	Reynolds averaged Navier–Stokes

References

1. Mao, S.; Zhou, T.; Wei, D.; Liu, W.; Zhang, Y. Heat transfer characteristics of supercritical water in channels: A systematic literature review of 20 years of research. *Appl. Therm. Eng.* **2021**, *197*, 117403. [CrossRef]
2. Nieuwenhuyse, J.N.; Lecompte, S.; Paepe, M.D. Current status of the thermohydraulic behavior of supercritical refrigerants: A review. *Appl. Therm. Eng.* **2023**, *218*, 119201. [CrossRef]
3. Sun, X.; Meng, H. Large eddy simulations and analyses of hydrocarbon fuel heat transfer in vertical upward flows at supercritical pressures. *Int. J. Heat Mass Transf.* **2021**, *170*, 120988. [CrossRef]
4. Li, L.; Jiang, W.-Q.; Li, Y.; Su, S.-Y.; Shi, J.-F.; Yang, F. Analysis and prediction of heat transfer deterioration of supercritical pressure cryogenic methane in a vertical tube. *Int. J. Heat Mass Transf.* **2021**, *180*, 121824. [CrossRef]
5. Xu, J.; Zhang, H.; Zhu, B.; Xie, J. Critical supercritical-boiling-number to determine the onset of heat transfer deterioration for supercritical fluids. *Sol. Energy* **2020**, *195*, 27–36. [CrossRef]
6. Rahman, M.M.; Dongxu, J.; Beni, M.S.; Hei, H.C.; He, W.; Zhao, J. Supercritical water heat transfer for nuclear reactor applications: A review. *Ann. Nucl. Energy* **2016**, *97*, 53–65. [CrossRef]
7. Schulenberg, T.; Leung, L.K.H.; Oka, Y. Review of R&D for supercritical water cooled reactors. *Prog. Nucl. Energy* **2014**, *77*, 282–299.
8. Bazargan, M.; Fraser, D. Heat Transfer to Supercritical Water in a Horizontal Pipe: Modeling, New Empirical Correlation, and Comparison Against Experimental Data. *J. Heat Transf.* **2009**, *131*, 061702. [CrossRef]
9. Pioro, I.L.; Duffey, R.B. Experimental heat transfer in supercritical water flowing inside channels (survey). *Nucl. Eng. Des.* **2005**, *235*, 2407–2430. [CrossRef]
10. Shitsi, E.; Debrah, S.K.; Agbodemegbe, V.Y.; Ampomah-Amoako, E. Flow Instability in Parallel Channels with Water at Supercritical Pressure: A Review. *World J. Eng. Technol.* **2018**, *6*, 128–160. [CrossRef]
11. Zhang, X.R.; Yamaguchi, H. An experimental study on evacuated tube solar collector using supercritical CO_2. *Appl. Therm. Eng.* **2008**, *28*, 1225–1233. [CrossRef]
12. He, J.C.; Dang, C.B.; Hihara, E. Experimental investigation of heat transfer to supercritical R245fa flowing vertically upward in a circular tube. *Int. J. Heat Mass Transf.* **2018**, *127*, 286–295. [CrossRef]
13. He, J.C.; Dang, C.B.; Hihara, E. Supercritical heat transfer characteristics of R1233zd(E) in vertically upward flow. *Int. J. Heat Mass Transf.* **2018**, *127*, 497–505. [CrossRef]
14. Tao, Z.; Cheng, Z.; Zhu, J.; Lin, D.; Wu, H. Large eddy simulation of supercritical heat transfer to hydrocarbon fuel. *Int. J. Heat Mass Transf.* **2018**, *121*, 1251–1263. [CrossRef]
15. Cheng, Z.; Tao, Z.; Zhu, J.; Wu, H. Diameter effect on the heat transfer of supercritical hydrocarbon fuel in horizontal tubes under turbulent conditions. *Appl. Therm. Eng.* **2018**, *134*, 39–53. [CrossRef]
16. Fu, Y.; Wen, J.; Tao, Z.; Xu, G.; Huang, H. Experimental research on convective heat transfer of supercritical hydrocarbon fuel flowing through U-turn tubes. *Appl. Therm. Eng.* **2017**, *116*, 43–55. [CrossRef]
17. Wen, J.; Huang, H.; Jia, Z.; Fu, Y.; Xu, G. Buoyancy effects on heat transfer to supercritical pressure hydrocarbon fuel in a horizontal miniature tube. *Int. J. Heat Mass Transf.* **2017**, *115*, 1173–1181. [CrossRef]
18. Urbano, A.; Nasuti, F. Conditions for the occurrence of heat transfer deterioration in light hydrocarbons flows. *Int. J. Heat Mass Transf.* **2013**, *65*, 599–609. [CrossRef]
19. Liu, X.; Xu, X.; Liu, C.; Ye, J.; Li, H.; Bai, W.; Dang, C. Numerical study of the effect of buoyancy force and centrifugal force on heat transfer characteristics of supercritical CO_2 in helically coiled tube at various inclination angles. *Appl. Therm. Eng.* **2017**, *116*, 500–515. [CrossRef]
20. Zhang, S.; Xu, X.; Liu, C.; Dang, C. A review on application and heat transfer enhancement of supercritical CO_2 in low-grade heat conversion. *Appl. Energy* **2020**, *269*, 114962. [CrossRef]
21. Xie, G.; Xu, X.; Lei, X.; Li, Z.; Li, Y.; Sunden, B. Heat transfer behaviors of some supercritical fluids: A review. *Chin. J. Aeronaut.* **2020**, *35*, 290–306. [CrossRef]
22. Xu, W.; Li, Y.; Wang, Y.; Li, M.; Zhao, J.; Li, M.; Tian, H. Experimental investigations on cooling heat transfer of CO_2-lubricant mixtures in horizontal tubes at supercritical pressure: A review. *Int. J. Refrig.* **2022**, *139*, 168–179. [CrossRef]
23. Shitsi, E.; Debrah, S.K.; Agbodemegbe, V.Y.; Ampomah-Amoako, E. Performance of Heat Transfer Correlations Adopted at Supercritical Pressures: A Review. *World J. Eng. Technol.* **2018**, *6*, 241–267. [CrossRef]
24. Tian, R.; Xu, Y.; Shi, L.; Song, P.; Wei, M. Mixed convection heat transfer of supercritical pressure R1234yf in horizontal flow: Comparison study as alternative to R134a in organic Rankine cycles. *Energy* **2020**, *205*, 118061. [CrossRef]
25. Lau, K.T.; Khan, S.A.; Eze, C.; Tan, B.; Zhao, J. Numerical investigation on deteriorated heat transfer of supercritical water flowing upward in tubes with variable cross-sectional geometries. *Int. Commun. Heat Mass Transf.* **2022**, *136*, 106203. [CrossRef]

26. Deev, V.; Kharitonov, V.; Baisov, A.; Churkin, A. Heat transfer characteristics of water under supercritical conditions. *Int. J. Therm. Sci.* **2022**, *171*, 107238. [CrossRef]
27. Gharehdaghi, S.; Moujaes, S.F.; Nejad, A. Thermal-fluid analysis of a parabolic trough solar collector of a direct supercritical carbon dioxide Brayton cycle: A numerical study. *Sol. Energy* **2021**, *220*, 766–787. [CrossRef]
28. Viswanathan, K.; Krishnamoorthy, G. The effects of wall heat fluxes and tube diameters on laminar heat transfer rates to supercritical CO_2. *Int. Commun. Heat Mass Transf.* **2021**, *123*, 105197. [CrossRef]
29. Zhao, H.J.; Li, X.W.; Wu, X.X. Numerical investigation of supercritical water turbulent flow and heat transfer characteris-tics in vertical helical tubes. *J. Supercrit. Fluids* **2017**, *127*, 48–61. [CrossRef]
30. Yang, M. Numerical study of the heat transfer to carbon dioxide in horizontal helically coiled tubes under supercritical pressure. *Appl. Therm. Eng.* **2016**, *109*, 685–696. [CrossRef]
31. Xu, X.; Liu, C.; Dang, C.; Wu, Y.; Liu, X. Experimental investigation on heat transfer characteristics of supercritical CO_2 cooled in horizontal helically coiled tube. *Int. J. Refrig.* **2016**, *67*, 190–201. [CrossRef]
32. Liu, X.X.; Xu, X.X.; Liu, C.; Bai, W.; Dang, C. Heat transfer deterioration in helically coiled heat exchangers in trans-critical CO_2 Rankine cycles. *Energy* **2018**, *147*, 1–14. [CrossRef]
33. Inagaki, Y.; Koiso, H.; Takumi, H.; Ioka, I.; Miyamoto, Y. Thermal hydraulic study on a high temperature gas gas-heat exchanger with heli-cally coiled tube bundles. *Nucl. Eng. Des.* **1998**, *185*, 141–151. [CrossRef]
34. Taklifi, A.; Aliabadi, A.; Hanafizadeh, P.; Akhavan-Behabadi, M.A. Effect of inclination on frictional pressure drop of supercritical water flows in internally ribbed tubes: An experimental study. *J. Supercrit. Fluids* **2017**, *125*, 56–65. [CrossRef]
35. Li, Z.; Wu, Y.; Tang, G.; Lu, J.; Wang, H. Numerical analysis of buoyancy effect and heat transfer enhancement in flow of supercriti-cal water through internally ribbed tubes. *Appl. Therm. Eng.* **2016**, *98*, 1080–1090. [CrossRef]
36. Xu, K.K.; Tang, L.J.; Meng, H. Numerical study of supercritical-pressure fluid flows and heat transfer of methane in ribbed cooling tubes. *Int. J. Heat Mass Transf.* **2015**, *84*, 346–358. [CrossRef]
37. Li, Z.; Wu, Y.; Tang, G.; Zhang, D.; Lu, J. Comparison between heat transfer to supercritical water in a smooth tube and in an inter-nally ribbed tube. *Int. J. Heat Mass Transf.* **2015**, *84*, 529–541. [CrossRef]
38. Li, Z.; Lu, J.; Tang, G.; Liu, Q.; Wu, Y. Effects of rib geometries and property variations on heat transfer to supercritical water in in-ternally ribbed tubes. *Appl. Therm. Eng.* **2015**, *78*, 303–314. [CrossRef]
39. Zhang, Q.; Li, H.; Zhang, W.; Li, L.; Lei, X. Experimental study on heat transfer to the supercritical water upward flow in a vertical tube with internal helical ribs. *Int. J. Heat Mass Transf.* **2015**, *89*, 1044–1053. [CrossRef]
40. Zdaniuk, G.J.; Chamra, L.M.; Mago, P.J. Experimental determination of heat transfer and friction in helically-finned tubes. *Exp. Therm. Fluid Sci.* **2008**, *32*, 761–775. [CrossRef]
41. Bae, Y.Y.; Kim, H.Y.; Yoo, T.H. Effect of a helical wire on mixed convection heat transfer to carbon dioxide in a vertical cir-cular tube at supercritical pressures. *Int. J. Heat Fluid Flow* **2011**, *32*, 340–351. [CrossRef]
42. Li, H.; Wang, H.; Luo, Y.; Gu, H.; Shi, X.; Chen, T.; Laurien, E.; Zhu, Y. Experimental investigation on heat transfer from a heated rod with a helically wrapped wire inside a square vertical channel to water at supercritical pressures. *Nucl. Eng. Des.* **2009**, *239*, 2004–2012. [CrossRef]
43. Liu, Z.-B.; He, Y.-L.; Qu, Z.-G.; Tao, W.-Q. Experimental study of heat transfer and pressure drop of supercritical CO_2 cooled in metal foam tubes. *Int. J. Heat Mass Transf.* **2015**, *85*, 679–693. [CrossRef]
44. Liu, Z.-B.; He, Y.-L.; Li, Y.-S.; Qu, Z.-G.; Tao, W.-Q. Heat transfer characteristics of supercritical CO2 flow in metal foam tubes. *J. Supercrit. Fluids* **2015**, *101*, 36–47. [CrossRef]
45. Yuan, Y.; Cao, J.; Wang, X.; Zhang, Z.; Liu, Y. Economic-effectiveness analysis of micro-fins helically coiled tube heat exchanger and optimization based on multi-objective differential evolution algorithm. *Appl. Therm. Eng.* **2022**, *201*, 117764. [CrossRef]
46. Fan, M.; Bao, Z.; Liu, S.; Huang, W. Flow and heat transfer in the eccentric annulus of the helically coiled tube-in-tube heat exchanger used in an aero-engine. *Int. J. Therm. Sci.* **2022**, *179*, 107636. [CrossRef]
47. Han, Y.; Zhang, C.-C.; Zhu, Y.-J.; Wu, X.-H.; Jin, T.-X.; Li, J.-N. Investigation of heat transfer Exergy loss number and its application in optimization for the shell and helically coiled tube heat exchanger. *Appl. Therm. Eng.* **2022**, *211*, 118424. [CrossRef]
48. Xu, R.N.; Luo, F.; Jiang, P.X. Experimental research on the turbulent convection heat transfer of supercritical pressure CO_2 in a serpentine vertical mini tube. *Int. J. Heat Mass Transf.* **2015**, *91*, 552–561. [CrossRef]
49. Zhang, W.; Wang, S.; Li, C.; Xu, J. Mixed convective heat transfer of CO_2 at supercritical pressures flowing upward through a vertical helically coiled tube. *Appl. Therm. Eng.* **2014**, *88*, 61–70. [CrossRef]
50. Li, Z.; Zhai, Y.; Bi, D.; Li, K.; Wang, H.; Lu, J. Orientation effect in helical coils with smooth and rib-roughened wall: Toward improved gas heaters for supercritical carbon dioxide Rankine cycles. *Energy* **2017**, *140*, 530–545. [CrossRef]
51. Zhang, C.; Wang, D.; Xiang, S.; Han, Y.; Peng, X. Numerical investigation of heat transfer and pressure drop in helically coiled tube with spherical corrugation. *Int. J. Heat Mass Transf.* **2017**, *113*, 332–341. [CrossRef]
52. Wang, K.-Z.; Xu, X.-X.; Liu, C.; Bai, W.-J.; Dang, C.-B. Experimental and numerical investigation on heat transfer characteristics of supercritical CO_2 in the cooled helically coiled tube. *Int. J. Heat Mass Transf.* **2017**, *108*, 1645–1655. [CrossRef]
53. Lazova, M.; Huisseune, H.; Kaya, A.; Lecompte, S.; Kosmadakis, G.; De Paepe, M. Performance Evaluation of a Helical Coil Heat Exchanger Working under Supercritical Conditions in a Solar Organic Rankine Cycle Installation. *Energies* **2016**, *9*, 432–452. [CrossRef]

54. Sun, X.; Yuan, Y.; Tan, T.; Jing, T.; Qin, F.; Meng, H. Large eddy simulations of heat transfer and thermal oxidative coking of aviation kerosene in vertical U-tube at a supercritical pressure. *Int. J. Heat Mass Transf.* **2022**, *195*, 123205. [CrossRef]
55. Wen, J.; Huang, H.; Fu, Y.; Xu, G.; Zhu, K. Heat transfer performance of aviation kerosene RP-3 flowing in a vertical helical tube at supercritical pressure. *Appl. Therm. Eng.* **2017**, *121*, 853–862. [CrossRef]
56. Xu, X.X.; Liu, X.X.; Liu, C.; Dang, C.B. Experimental Study On Heat Transfer Of Supercritical CO_2 Cooled In Horizontal Helically Coiled Tube. In Proceedings of the 9th Asian Conference on Refrigeration and Air Conditioning, Sapporo, Japan, 10–13 June 2018.
57. Xu, X.; Zhang, Y.; Liu, C.; Zhang, S.; Dang, C. Experimental investigation of heat transfer of supercritical CO_2 cooled in helically coiled tubes based on exergy analysis. *Int. J. Refrig.* **2018**, *89*, 177–185. [CrossRef]
58. Hardik, B.K.; Baburajan, P.K.; Prabhu, S.V. Local heat transfer coefficient in helical coils with single phase flow. *Int. J. Heat Mass Transf.* **2015**, *89*, 522–538. [CrossRef]
59. Xu, R.N.; Luo, F.; Jiang, P.X. Buoyancy effects on turbulent heat transfer of supercritical CO_2 in a vertical mini-tube based on continuous wall temperature measurements. *Int. J. Heat Mass Transf.* **2017**, *110*, 576–586. [CrossRef]
60. Xu, J.; Yang, C.; Zhang, W.; Sun, D. Turbulent convective heat transfer of CO_2 in a helical tube at near-critical pressure. *Int. J. Heat Mass Transf.* **2015**, *80*, 748–758. [CrossRef]
61. Yang, D.; Xie, J.; Lv, J.; Wang, J. An Experimental and Numerical Study of Helix Tube Gas Cooler for Super-Critical Carbon Dioxide. *J. Chem. Eng. Jpn.* **2017**, *50*, 900–908. [CrossRef]
62. Liu, X.; Xu, X.; Liu, C.; He, J.; Dang, C. The effect of geometry parameters on the heat transfer performance of supercritical CO_2 in hori-zontal helically coiled tube under the cooling condition. *Int. J. Refrig.* **2019**, *106*, 650–661. [CrossRef]
63. Wang, M.; Zheng, M.; Wang, R.; Tian, L.; Ye, C.; Chen, Y.; Gu, H. Experimental studies on local and average heat transfer characteristics in helical pipes with single phase flow. *Ann. Nucl. Energy* **2019**, *123*, 78–85. [CrossRef]
64. Wang, R.T.; Zhao, J.J.; Bao, Z.W. Thermal cracking and coke deposition characteristics of aviation kerosene RP-3 in an S-bend tube. *Fuel* **2022**, *313*, 122673. [CrossRef]
65. Lei, Z.L.; Bao, Z.W. Experimental investigation on laminar heat transfer performances of RP-3 at supercritical pressure in the helical coiled tube. *Int J Heat Mass Transf.* **2022**, *185*, 122326. [CrossRef]
66. Han, Z.; Zhou, W.; Zhao, X.; Zhang, M. Thermal oxidation deposition characteristics of RP-3 kerosene in serpentine tubes under supercritical pressure. *Fuel* **2022**, *3105*, 122369. [CrossRef]
67. Chang, F.; Hu, H.; Shang, Y.; Hu, Y.; Li, X.; Lei, H.; Li, H. Experimental and numerical study on the heat transfer characteristic of supercritical water with high mass velocity in a helically coiled tube. *Int J Heat Mass Transf.* **2022**, *197*, 123320. [CrossRef]
68. Liu, X.; Xu, X.; Jiao, Y.; He, C.; Liu, L.; Dang, C. Flow structure with mixed turbulent flow of supercritical CO_2 heated in helically coiled tube. *Appl. Therm. Eng.* **2021**, *189*, 116684. [CrossRef]
69. Zheng, Y.; Jiang, P.-X.; Luo, F.; Xu, R.-N. Instability during transition to turbulence of supercritical pressure CO_2 in a vertical heated serpentine tube. *Int. J. Therm. Sci.* **2019**, *145*, 105976. [CrossRef]
70. Fu, Y.; Xu, G.; Wen, J.; Huang, H. Thermal oxidation coking of aviation kerosene RP-3 at supercritical pressure in helical tubes. *Appl. Therm. Eng.* **2018**, *128*, 1186–1195. [CrossRef]
71. Pei, X.Y.; Hou, L.Y. Secondary flow and oxidation coking deposition of aviation fuel. *Fuel* **2016**, *167*, 68–74. [CrossRef]
72. Wang, K.; Xu, X.; Wu, Y.; Liu, C.; Dang, C. Numerical investigation on heat transfer of supercritical CO_2 in heated helically coiled tubes. *J. Supercrit. Fluid* **2015**, *99*, 112–120. [CrossRef]
73. Ren, Z.; Zhao, C.-R.; Jiang, P.-X.; Bo, H.-L. Investigation on local convection heat transfer of supercritical CO2 during cooling in horizontal semicircular channels of printed circuit heat exchanger. *Appl. Therm. Eng.* **2019**, *157*, 113697. [CrossRef]
74. Wang, J.; Guan, Z.; Gurgenci, H.; Hooman, K.; Veeraragavan, A.; Kang, X. Computational investigations of heat transfer to supercritical CO_2 in a large horizontal tube. *Energ Convers. Manag.* **2018**, *157*, 536–548. [CrossRef]
75. Eze, C.; Lau, K.T.; Ahmad, S.; Nnamani, N.; Ferrand, T.; Gschnaidtner, T.; Wieland, C.; Zhao, J. Mitigation of heat transfer deterioration in a circular tube with supercritical CO_2 using a novel small-scale multiple vortex generator. *Int. J. Therm. Sci.* **2020**, *156*, 106481. [CrossRef]
76. Eze, C.; Wong, K.W.; Gschnaidtne, T.; Cai, J.; Zhao, J. Numerical study of effects of vortex generators on heat transfer deterioration of supercritical water upward flow. *Int J Heat Mass Transf.* **2019**, *137*, 489–505. [CrossRef]
77. Zhang, Y.; Yao, Y.; Li, Z.; Tang, G.; Wu, Y.; Wang, H.; Lu, J. Low-grade heat utilization by supercritical carbon dioxide Rankine cycle: Analysis on the performance of gas heater subjected to heat flux and convective boundary conditions. *Energ Convers. Manag.* **2018**, *162*, 39–54. [CrossRef]
78. Liang, J.H.; Liu, Z.Q.; Pan, Y. Coupled Heat Transfer of Supercritical n-Decane in a Curved Cooling Channel. *J. Thermophys. Heat Transf.* **2016**, *30*, 635–641. [CrossRef]
79. Li, Z.; Zhai, Y.; Li, K.; Wang, H.; Lu, J. A quantitative study on the interaction between curvature and buoyancy effects in helically coiled heat exchangers of supercritical CO_2 Rankine cycles. *Energy* **2016**, *116*, 661–676. [CrossRef]
80. Wang, C.; Sun, B.; Lin, W.; He, F.; You, Y.; Yu, J. Turbulent convective heat transfer of methane at supercritical pressure in a helical coiled tube. *J. Therm. Sci.* **2018**, *27*, 55–63. [CrossRef]
81. Li, L.J. Turbulent heat transfer to near-critical water in a heated curved pipe under the conditions of mixed convection. *Int. J. Heat Mass Transf.* **1998**, *42*, 3147–3158. [CrossRef]
82. Li, X.; Zhong, F.; Fan, X.; Huai, X.; Cai, J. Study of turbulent heat transfer of aviation kerosene flows in a curved pipe at supercritical pressure. *Appl. Therm. Eng.* **2010**, *30*, 1845–1851. [CrossRef]

83. Yang, M. Numerical study of the characteristic influence of the helically coiled tube on the heat transfer of carbon dioxide. *Appl. Therm. Eng.* **2016**, *102*, 882–896. [CrossRef]
84. Han, C.-L.; Ren, J.-J.; Dong, W.-P.; Bi, M.-S. Numerical investigation of supercritical LNG convective heat transfer in a horizontal ser-pentine tube. *Cryogenics* **2016**, *78*, 1–13. [CrossRef]
85. Yakhot, V.; Orszag, S.A. Renormalization group analysis of turbulence: I. Basic theory. *J. Sci. Comput.* **1986**, *1*, 1–51. [CrossRef]
86. Cui, X.; Guo, J.; Huai, X.; Zhang, H.; Cheng, K.; Zhou, J. Numerical investigations on serpentine channel for supercritical CO_2 recuperator. *Energy* **2019**, *172*, 517–530. [CrossRef]
87. Dang, C.B.; Hihara, E. In-tube cooling heat transfer of supercritical carbon dioxide. Part 2. Comparison of numerical calculation with different turbulence models. *Int. J. Refrig.* **2004**, *27*, 748–760. [CrossRef]
88. Xu, C.; Laurien, E. Flow stratification of supercritical CO_2 in a heated horizontal pipe. *J. Supercrit. Fluids* **2016**, *116*, 172–189.
89. Pandey, S.; Xu, C.; Laurien, E. Investigation of in-tube cooling of carbon dioxide at supercritical pressure by means of direct numerical simulation. *Int J Heat Mass Transf.* **2017**, *114*, 944–957. [CrossRef]
90. Kim, W.S.; He, S.; Jackson, J.D. Assessment by comparison with DNS data of turbulence models used in simulations of mixed convection. *Int J Heat Mass Transf.* **2008**, *51*, 1293–1312. [CrossRef]
91. Zhao, Z.; Che, D.; Zhang, Y.; Yao, S.; Zhang, K.; Lin, Y. Numerical investigation on conjugate heat transfer to supercritical CO_2 in membrane helical coiled tube heat exchangers. *Numer. Heat Transf. Part A Appl.* **2016**, *69*, 977–995. [CrossRef]
92. Zhang, S.; Xu, X.; Liu, C.; Zhang, Y.; Dang, C. The buoyancy force and flow acceleration effects of supercritical CO_2 on the turbulent heat transfer characteristics in heated vertical helically coiled tube. *Int. J. Heat Mass Transf.* **2018**, *125*, 274–289. [CrossRef]
93. Ciofalo, M.; Arini, A.; Liberto, M.D. On the influence of gravitational and centrifugal buoyancy on laminar flow and heat transfer in curved pipes and coils. *Int. J. Heat Mass Transf.* **2015**, *82*, 123–134. [CrossRef]
94. Yi, Z.M.; Xu, Y.; Chen, X.L. Numerical study on heat transfer characteristics of supercritical CO_2 in a vertical heating serpentine micro-tube. *Appl. Therm. Eng.* **2022**, *212*, 118609. [CrossRef]
95. Li, Y.X.; Diao, L.; Chen, Y. Numerical simulation on heat transfer of supercritical carbon dioxide in helical coiled channels under one-side heating. *Int. J. Sci.* **2022**, *174*, 107391. [CrossRef]
96. Jiang, Y.-R.; Hu, P.; Jia, C.-Q.; Zhao, P.-P.; Jia, L. Analysis of supercritical heat transfer in horizontal helical tube with internal roughness. *Appl. Therm. Eng.* **2022**, *211*, 118463. [CrossRef]
97. Jiang, Y.R.; Hu, P. Analysis of Heat Transfer Oscillation and Buoyancy Effects of Supercritical R1234ze(E) Cooled in Horizontal Helically Coiled Tubes. *J. Sci. Eng. Appl.* **2021**, *13*, 061012. [CrossRef]
98. Huang, Y.; Duan, L.; Liu, D.; Wang, Y. Computational investigation on heat transfer of supercritical CO_2 in horizontal U-tubes. *J. Supercrit. Fluids* **2022**, *188*, 105690. [CrossRef]
99. Luo, W.; Han, H.; Yu, R.; Cai, L.; Gao, R. Flow and heat transfer characteristics of air and n-decane in eccentric tube-in-tube helically coiled heat exchangers. *Int. J. Therm. Sci.* **2021**, *170*, 107170. [CrossRef]
100. Bai, J.; Pan, J.; Wang, W.; Wang, K.; Wu, G. Ice formation prediction and heat transfer analysis of LNG in serpentine tube under supercritical pressure. *Int. J. Therm. Sci.* **2020**, *149*, 106137. [CrossRef]
101. Zhang, S.; Xu, X.; Liu, C.; Liu, X.; Zhang, Y.; Dang, C. The heat transfer of supercritical CO_2 in helically coiled tube: Trade-off between curvature and buoyancy effect. *Energy* **2019**, *176*, 765–777. [CrossRef]
102. Li, F.B.; Bai, B.F. Flow and heat transfer of supercritical water in the vertical helically-coiled tube under half-side heating condition. *Appl. Therm. Eng.* **2018**, *133*, 512–519. [CrossRef]
103. Dean, W.R. Note on the Motion of_Fluid in a Curved Pipe. *Lond. Edinb. Dublin Philos. Mag. J. Sci.* **1927**, *4*, 208–223. [CrossRef]
104. Chen, W.; Yang, Z.; Yang, L.; Chyu, M.K. Numerical Investigation of Heat Transfer and Flow Characteristics of Supercritical CO_2 in U-Duct. *Appl. Therm. Eng.* **2018**, *144*, 532–539. [CrossRef]
105. Huang, D.; Li, W. A brief review on the buoyancy criteria for supercritical fluids. *Appl. Therm. Eng.* **2018**, *131*, 977–987. [CrossRef]
106. Qiu, Y.; Li, M.-J.; He, Y.-L.; Tao, W.-Q. Thermal performance analysis of a parabolic trough solar collector using supercritical CO_2 as heat transfer fluid under non-uniform solar flux. *Appl. Therm. Eng.* **2016**, *115*, 1255–1265. [CrossRef]
107. Rao, N.T.; Oumer, A.N.; Jamaludin, U. State-of-the-art on flow and heat transfer characteristics of supercritical CO_2 in various channels. *J. Supercrit. Fluids* **2016**, *116*, 132–147. [CrossRef]
108. Huang, D.; Wu, Z.; Sunden, B.; Li, W. A brief review on convection heat transfer of fluids at supercritical pressures in tubes and the recent progress. *Appl. Energy* **2016**, *162*, 494–505. [CrossRef]
109. Yildiz, S.; Groeneveld, D.C. Diameter effect on supercritical heat transfer. *Int. Commun. Heat Mass* **2014**, *54*, 27–32. [CrossRef]
110. Jackson, J.D.; Cotton, M.A.; Axcell, B.P. Studies of mixed convection in vertical tubes. *Int. J. Heat Fluid Flow* **1988**, *10*, 2–15. [CrossRef]
111. Jackson, J.D. Influences of buoyancy and thermal boundary conditions on heat transfer with naturally-induced flow. In Proceedings of the International Heat Transfer Conference 12, Grenoble, France, 18–23 August 2002.
112. Kurganov, V.A.; Kaptil, A.G. Velocity and Enthalpy Fields and Eddy Diffusivities in a Heated Supercritical Fluid Flow. *Exp. Therm. Fluid Sci.* **1992**, *5*, 465–478. [CrossRef]
113. Bae, J.H.; Yoo, J.Y.; Choi, H. Direct numerical simulation of turbulent supercritical flows with heat transfer. *Phys. Fluids* **2005**, *17*, 105104. [CrossRef]
114. Pandey, S.; Laurien, E.; Xu, C. A modified convective heat transfer model for heated pipe flow of supercritical carbon diox-ide. *Int. J. Therm. Sci.* **2017**, *117*, 227–238. [CrossRef]

115. Pandey, S.; Laurien, E. Heat transfer analysis at supercritical pressure using two-layer theory. *J. Supercrit. Fluids* **2016**, *109*, 80–86. [CrossRef]
116. Hiroaki, H.; Tsuge, A.; Hirata, M.; Nishiwaki, N. Effects of buoyancy and of acceleration owing to thermal expansion on forced turbulent convection in vertical circular tubes-criteria of the effects, velocity and temperature profiles, and reverse transition form turbu-lent to laminar flow. *Int. J. Heat Mass Transf.* **1973**, *16*, 1267–1288. [CrossRef]
117. Yao, L.S.; Berger, S. Flow in_heated curved pipes. *J. Fluid Mech.* **1977**, *88*, 339–354. [CrossRef]
118. Petukhov, B.S.; Kuleshov, V.A.; Sheckter, Y.L. Turbulent Flow and Heat Transfer in Horizontal Tubes with Substantial Influence of Thermogravitational Forces. In Proceedings of the International Heat Transfer Conference Digital Library. Begel House Inc, Tokyo, Japan, 3–7 September 1974.